Moore, J. C., Mascle, A., et al., 1990
Proceedings of the Ocean Drilling Program, Scientific Results, Vol. 110

5. EOCENE-OLIGOCENE SEDIMENTATION IN THE TIBURON RISE/ODP LEG 110 AREA: AN EXAMPLE OF SIGNIFICANT UPSLOPE FLOW OF DISTAL TURBIDITY CURRENTS[1]

James F. Dolan,[2,3] Christian Beck,[4,5] Yujiro Ogawa,[6] and Adam Klaus[7,8]

ABSTRACT

One of the most surprising results from ODP Leg 110 was the discovery of a 220-m-thick sequence of anomalously coarse-grained sediments on the slope of the Tiburon Rise, an area in which we had expected to encounter only hemipelagic and pelagic deposits. This middle Eocene-upper Oligocene sequence consists of 37% mud, silt, and sand terrigenous turbidites, 10% marl turbidites that may have been derived from either South America or from higher on the Tiburon Rise, and 53% hemipelagic "background" clays deposited below the CCD. The terrigenous beds are located approximately 1100 km from their source, yet they were deposited on the slope of the rise at least 800 m above the adjacent abyssal plain. These deposits thus represent an exceptional example of upslope deposition of distal turbidity currents. Two major terrigenous sediment pulses (late middle Eocene and late early Oligocene) probably resulted from increased sediment supply caused by tectonic movements of the northern South American borderland, rather than from eustatic sea-level effects. The oil-bearing Scotland Group sandstones of Barbados are approximately the same age as the Leg 110 terrigenous turbidites, and they may have been deposited in response to the same tectonic events. However, the Scotland Group sandstones had a predominantly cratonic source, whereas the Leg 110 deposits were probably derived from a more easterly, mixed cratonic-shelfal source.

INTRODUCTION

Leg 110 of the Ocean Drilling Program (ODP) consisted of an E–W transect of seven sites across the toe of the northern Lesser Antilles accretionary prism (Figs. 1, 2). These sites were drilled in the vicinity of the Tiburon Rise, a WNW–ESE trending basement ridge that is presently being underthrust beneath the accretionary prism (Figs. 1, 2). ODP Site 672 was drilled as an oceanic reference site on the slope of the rise, 5 km to the east of the accretionary prism deformation front (Fig. 2). The predominance of hemipelagic and pelagic deposits at Site 672 reflects the mid-ocean position of the Tiburon Rise, which is located more than 1100 km from South American sediment sources (Fig. 1). This distance has not changed through time, because the Tiburon Rise lies on the South American-south Atlantic Plate, and has therefore not migrated with respect to South America. Some volcaniclastic silt and sand presently reach the Leg 110 area from eruptions of the Lesser Antilles island arc to the west. However, regional plate reconstructions indicate that during Paleogene time the island arc lay far to the west of its present position (Pindell and Barrett, in press), and no significant ash reached the area until late Oligocene time (see Site 672, Mascle, Moore, et al., 1988). Consequently, one of the most surprising results of Leg 110 was the discovery of a 220-m-thick, middle Eocene to upper Oligocene section rich in terrigenous sand, silt and mud on the slope of the Tiburon Rise. This paper will focus on the origin, regional significance, and sea-level vs. tectonic controls on deposition of these sediments.

THE TIBURON RISE: EVIDENCE FOR SHALLOW BATHYMETRY DURING PALEOGENE TIME

Because this paper focuses on upslope deposition of turbidity currents, it is essential that the paleobathymetry of the Leg 110 area be accurately established. The Tiburon Rise is a bathymetric ridge that presently stands as high as 1500 m above the surrounding abyssal plain (Fig. 2). This ridge is one of a series of E–W to WNW–ESE trending ridges and troughs that characterize the west-central Atlantic Ocean (Figs. 1, 3; Peter and Westbrook, 1976). These features are thought to be associated with oceanic fracture zones that developed during opening of the central Atlantic during Senonian (Late Cretaceous) time (Westbrook et al., 1984a).

Maps of depth to acoustic basement derived from seismic reflection profiles show that the west-central Atlantic basement ridges and troughs are laterally discontinuous features that typically exhibit marked elevation changes along strike (Fig. 3; Westbrook et al., 1984b). These basement maps show that, east of 58°05′ W, the Tiburon Rise is bounded on the south by a deep trough that is filled by as much as 3 km of sediment (Fig. 3; Westbrook et al., 1984b). Unfortunately, the basement bathymetry to the southwest of the Tiburon Rise (west of 58°05′ W) remains poorly constrained because of poor seismic reflection coverage, which results from the westward thickening of the accretionary prism. However, seismic reflection profiles that cross the southeastern and northern margins of the Tiburon Rise, coupled with profiles from the structurally similar Barracuda Ridge to the north, provide considerable information about the age of the basement ridges and the paleobathymetry of the area.

Specifically, a NNE–SSW single-channel profile that crosses both the western Tiburon Rise and the central Barracuda Ridge (*Conrad* Line 1701, unpublished data; Mauffret et al., 1984) reveals onlap of sedimentary strata against the basement of both bathymetric ridges throughout most, if not all, of the sedimentary sections adjacent to the ridges. Similarly, a multi-channel seismic reflection profile collected by G. K. Westbrook along the southeastern margin of the rise shows probable onlap of the

[1] Moore, J. C., Mascle, A., et al., 1990. *Proc. ODP, Sci. Results*, 110: College Station, TX (Ocean Drilling Program).
[2] Earth Sciences Board, University of California, Santa Cruz, CA 95064.
[3] Present address: U.S. Geological Survey, M.S. 999, 345 Middlefield Road, Menlo Park, CA 94025.
[4] Department des Sciences de la Terre, Université de Lille, 59655 Villenueve d'Ascq Cedex, France.
[5] Present address: Sciences de la Terre, C.N.R.S., U.R.A. 694, Université de Savoie, B.P. 1104, Chambéry Cedex, France.
[6] Department of Geology, Faculty of Science, Kyushu University 33, Hakozaki, Fukuoka 812, Japan.
[7] Moss Landing Marine Laboratories, Moss Landing, CA 95039.
[8] Present Address: Hawaii Institute for Geophysics, 2525 Correa Road, University of Hawaii, Honolulu, HA 96822.

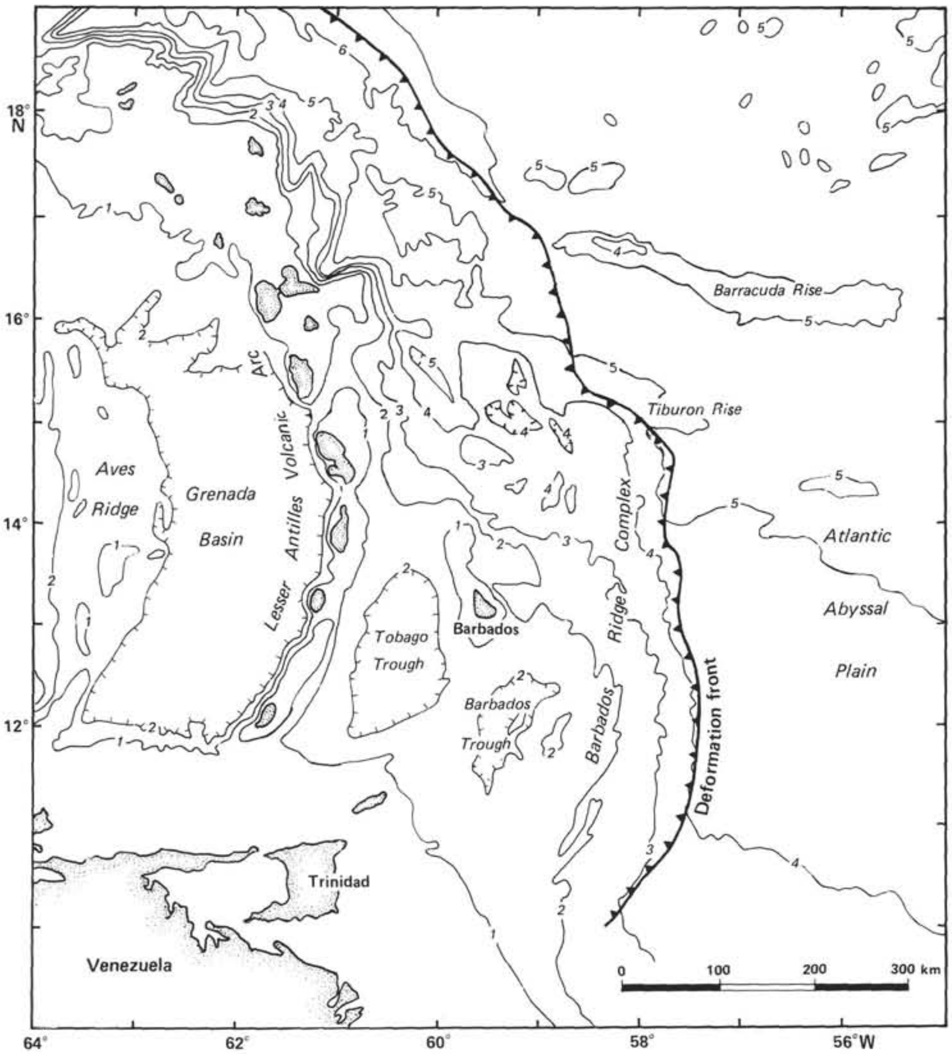

Figure 1. Location map of the eastern Caribbean/western Atlantic region showing the Tiburon Rise and Barbados. Depth in kilometers.

Tiburon Rise by the oldest part of the overlying sedimentary section (*Discovery* Cruise 109, Lines 12–14; unpublished data). These observations indicate that the ridges and troughs of the west-central Atlantic have existed as bathymetrically shallow features since soon after Late Cretaceous deposition of the oceanic basement in this region.

Accurate paleobathymetric reconstructions depend on the ability to successfully filter out recent uplift and subsidence. This problem is particularly important in the Tiburon Rise case because of the location of the rise on the downgoing (Atlantic) Plate at the front of the Lesser Antilles accretionary prism. As an oceanic fracture zone ridge enters a subduction zone, newly imposed stresses may reactivate ancient, extinct, ridge-bounding faults (e.g., Hilde et al., 1985; Bourgois et al., 1988). This phenomenon might result in erroneous estimates of paleo-relief of the bathymetric ridge.

Fortunately, this does not appear to be a major problem in the Tiburon Rise area. Seismic reflection profiles reveal only minor recent fault activity along the margins of both the Tiburon Rise and Barracuda Ridge; recent fault-related uplift accounts for only a small proportion of total ridge basement relief (generally <10% on most profiles). For example, a N-S profile along 56°30′ W (Peter and Westbrook, 1976; their Fig. 15) shows that the deep trough along the southern margin of the Tiburon Rise (Fig. 3) exhibits no recent fault control and indicates that in this area apparently all of the basement relief of the rise has existed since soon after basement deposition. This profile does show some recent normal faulting along the southern margin of the Barracuda Ridge to the north, which has increased basement relief of that ridge by approximately 7%–13%. Similarly, a parallel N-S profile to the east (along 54°30′ W) shows relatively recent normal fault activity that has increased total basement relief along the southern margin of the Barracuda Ridge by approximately 10% (Peter and Westbrook, 1976; their Fig. 17). *Conrad* Line 1701 shows only one possible recent normal fault located approximately 10 km north of the northern margin of the Tiburon Rise. Down-to-the-south offset on this fault represents only about 2%–3% of the total basement relief of the rise, and has actually caused an overall decrease in basement relief.

Multi-channel reflection profile CRV 128, which runs E-W along the western Tiburon Rise and across the toe of the accretionary prism (along 15°32′N), provides a more detailed picture of the timing of basement uplift (Shipboard Scientific Party, 1988). This line obliquely crosses nine, NW-SE and NE-SW trending normal faults that offset basement (see Site 671 report,

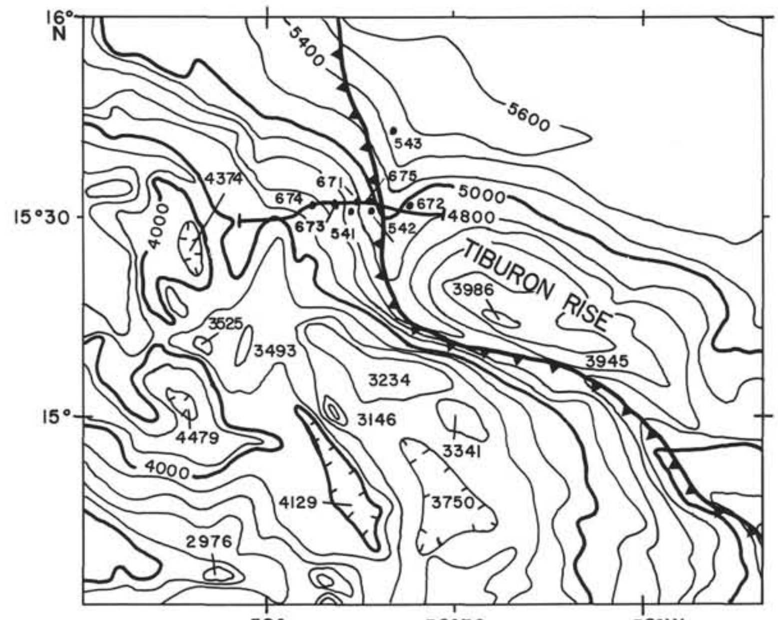

Figure 2. Location map of the Tiburon Rise/ODP Leg 110 area. Note ODP and DSDP sites as well as the location of seismic reflection profile CRV 128. Toothed line represents the deformation front of the Lesser Antilles accretionary prism.

Mascle, Moore, et al., 1988). Only one of these faults exhibits any recent minor activity. Four of the faults offset only Upper Cretaceous (and possibly Paleocene?) strata. The remaining four faults exhibit offsets that decrease with time, with most offset concentrated in the Upper Cretaceous-Paleocene section. Offsets diminish in middle and upper Eocene deposits, and a prominent latest Eocene/earliest Oligocene reflector is only slightly offset. Most fault activity therefore appears to have been associated with the early stages of the history of this portion of the Atlantic Basin (Mascle, Moore, et al., 1988).

The observations discussed above show that recent faulting has caused only minor changes in the basement relief of the Tiburon Rise, indicating that the rise had acquired almost all of its present basement relief by middle- or late Eocene time. Furthermore, depth-to-basement maps and evidence of sedimentary onlap of the ridges discussed above show that the rise has existed in essentially the same morphology and geographic position since Late Cretaceous time (compare Figs. 2 and 3).

LITHOLOGY

At ODP Site 672, the interval containing the anomalously coarse-grained terrigenous sediment is approximately 220 m thick and ranges in age from middle Eocene to late Oligocene (Fig. 4). The recovered sequence comprises three sediment types: Green clay, redeposited marl, and terrigenous mud, silt, and sand. Similar lithologies were recovered from several other ODP Leg 110 sites (e.g., Sites 671, 674), but the stratigraphic section at Site 672 is the most complete because of the absence of accretionary prism deformation. Consequently, the following discussion will focus on data from Site 672.

GREEN CLAYS: OBSERVATIONS

Green clays make up approximately 53% of the section and occur in intervals that range in thickness from < 1 cm to 360 cm (Fig. 5). These clays are typically featureless, although faint burrow mottles (*Planolites*?) occur locally. Most of the clay beds are non-calcareous, with local slightly calcareous intervals and rare highly calcareous intervals. Maximum CO_3 content measured was 60%. Grain-size analyses of 23 samples from clay beds indicate a grain-size range from 6.6–7.1 phi (very fine silt).

INTERPRETATION OF DEPOSITIONAL ENVIRONMENT

We interpret the green clays as hemipelagic "background" sediments (Fig. 6A). The massive, featureless nature of these deposits suggests that all primary sedimentary features have been completely obliterated during bioturbation. The non-calcareous composition of most of the clay beds indicates deposition below the carbonate compensation depth (CCD). We speculate that the minor calcareous component of these beds may be exotic material derived from higher on the rise, in an area located above the CCD (Fig. 6A). Alternatively, these local, slightly calcareous intervals may have been deposited when the CCD was slightly deeper. This interpretation implies deposition of the green clays near the CCD, at a depth where slight perturbations in the CCD resulted in a transition from non-calcareous to calcareous clay deposition. The rare, highly calcareous intervals probably represent texturally unrecognizable influxes of calcareous pelagic sediment, derived from either higher on the Tiburon Rise or from South America.

TERRIGENOUS MUDS, SILTS, AND SANDS: OBSERVATIONS

Due to the great distance of the Tiburon Rise from terrigenous sediment sources (i.e., South America and the Lesser Antilles Island Arc) during Eocene-Oligocene time, we had expected to encounter only pelagic and hemipelagic deposits in the mid-late Tertiary portion of Site 672. Consequently, we were surprised to observe that approximately 37% of the mid-late Tertiary section consists of anomalously coarse-grained terrigenous muds, silts, and sands (Fig. 5). At least 258 of these terrigenous beds occur within the middle Eocene-upper Oligocene interval at Site 672. No similar terrigenous beds were observed in sediments younger than late Oligocene. Siltstones and mud-

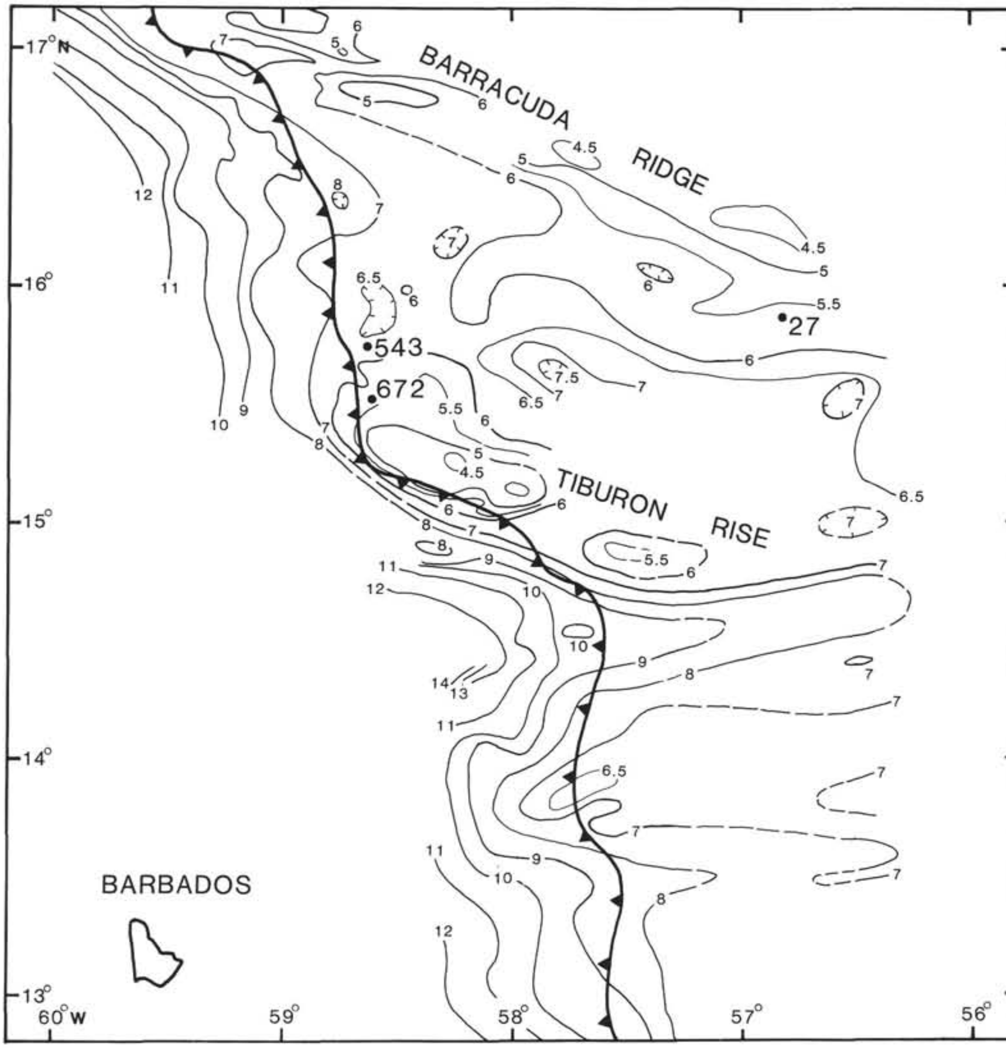

Figure 3. Contour map of depth to acoustic basement in the central western Atlantic region showing location of ODP Site 672 and DSDP Sites 27 and 543 (after Westbrook et al., 1984b). Depth in kilometers; selected half-kilometer contours also shown. Note that the alternating E-W basins and ridges in this region exhibit marked, along-strike changes in elevation. Toothed line represents deformation front of the Lesser Antilles accretionary prism. Compare with present bathymetry shown in Figure 2.

stones are the most common lithologies, especially in the Oligocene section, with an increasing percentage of sandstone downsection. Bed thicknesses range from <1 cm to 150 cm.

These terrigenous beds exhibit a wide range of compositions, varying from nearly pure detrital quartz to >80% planktonic foraminifers (Figs. 7A, 7B). However, most beds consist of a mixture of these two compositional end members. The most common sediment type consists of alternating 1- to 5-mm-thick carbonate-rich and quartz-rich laminae (Fig. 7C). The carbonate-rich laminae contain planktonic foraminifera, dark-colored micritic clasts, and abundant glauconite (Fig. 7C). Many of the foraminifer tests are filled with glauconite and pyrite. Ouartz-rich layers locally contain minor microcline, plagioclase, and glauconite, as well as rare glaucophane, zircon, clinopyroxene, and muscovite (Fig. 7A).

The olive-gray to dark gray terrigenous beds typically exhibit a sharp, flat base, and many beds grade smoothly upward into green clay intervals, although sharp upper contacts are also common (e.g., Figs. 8A, 8E). Most of the terrigenous beds exhibit either horizontal laminations or low-angle cross stratification (typically 2°–15° dip; Figs. 8A, 8B, 8D). Larger-scale (7 cm), higher-angle (15°–45°; possibly partially slumped?) cross bedding is limited to only a few examples (Fig. 8C). Many beds contain a thin basal silt lag, or several thin, silt laminations near the base of the bed. In addition, many beds exhibit decreasing intensity of planar laminations upcore, as well as an upcore decrease in the number of silt laminations. Crude mesoscopic graded bedding was also commonly observed.

Detailed grain-size analyses of 84 samples from 16 terrigenous beds and adjacent clay beds confirm the common occurrence of graded bedding (Fig. 9). Many of these graded beds were not detected during shipboard visual core inspection due to their fine grain sizes (Appendix). Phi sizes of the terrigenous beds on which we conducted grain-size analyses range from 3.45 (very fine sand) to 7.05 (very fine silt). However, we also recovered several coarser-grained beds (up to medium sand) on which we did not conduct grain-size analyses; three beds contained rare, coarse sand grains. Grain-size distributions in the terrigenous beds typically show a large mode in the coarse-silt fraction (Appendix). In contrast, adjacent hemipelagic clays show a large mode in the fine silt fraction.

Sand is more abundant in the Eocene portion of the mid-late Tertiary interval at Site 672. Much of the increased sand-sized component in the basal portion of the sequence consists of

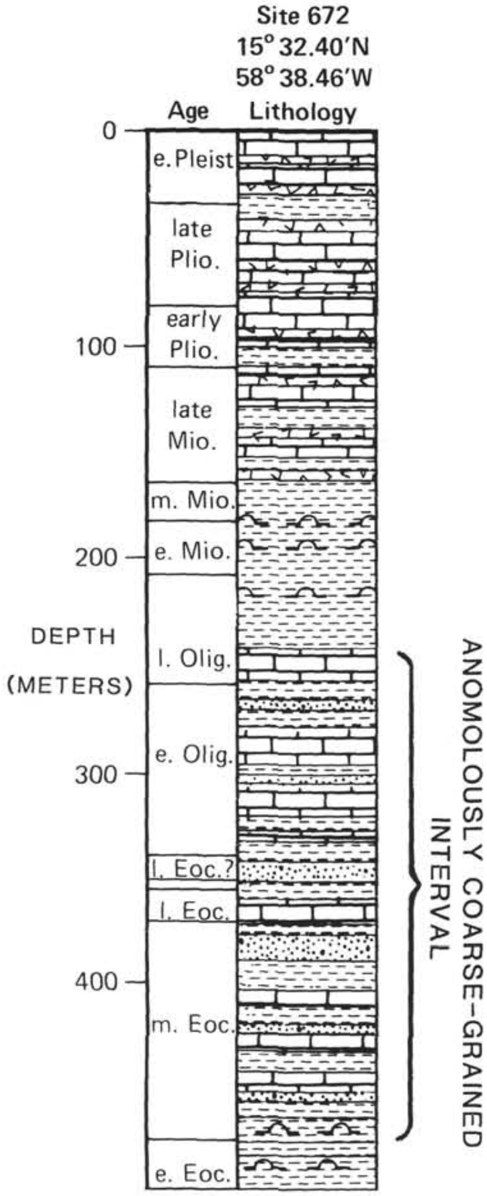

Figure 4. Stratigraphic column for ODP Site 672 showing the middle Eocene–upper Oligocene, anomalously coarse-grained interval.

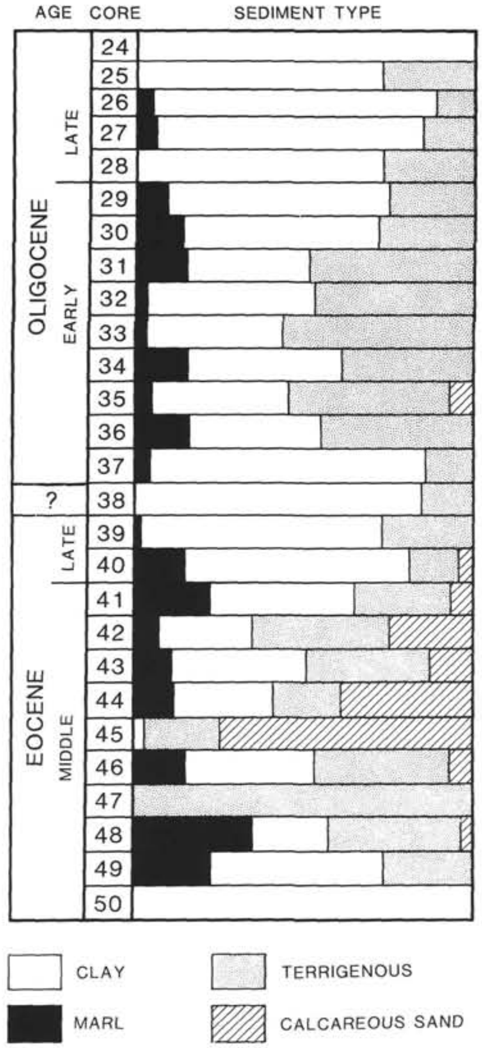

Figure 5. Histogram showing sediment types from the anomalously coarse-grained mid-late Tertiary section at Site 672. Note the presence of abundant calcareous sand in the Eocene portion of the interval.

glauconite- and foraminifera-rich sediment (Fig. 5). These gray-green, olive, and olive-gray sandstones and siltstones commonly grade upward into pale green marl beds. In many cases the beds are separated by an interval of pale green, highly calcareous, foraminifer-rich sand.

INTERPRETATION OF DEPOSITIONAL ENVIRONMENT

The composition of the Leg 110 silts and sands indicates derivation from South America, the nearest plausible source for the quartz, microcline, and glaucophane grains. The quartz was probably derived from the Guyana shield, whereas the glaucophane indicates an orogenic source area, possibly the Caribbean Mountain System of northern Venezuela (Beck et al., this volume). We interpret the glauconite-rich foraminifer sands as products of the northern South American shelf, possibly derived from the middle Eocene Caratas Formation of northern Venezuela, which consists largely of glauconitic, foraminifer-rich sediments (Beck et al., this volume).

The mode of deposition of these beds was the subject of lively debate during ODP Leg 110. It seemed reasonable that the terrigenous sediments were derived from South America and that they had reached the Tiburon Rise area as distal turbidity currents. However, we were uncertain as to their final mode of deposition on the slopes of the Tiburon Rise. As discussed above, probable Late Cretaceous sedimentary onlap indicates that the rise was a positive bathymetric feature prior to deposition of the anomalously coarse-grained section, ruling out deposition of the terrigenous beds as distal, abyssal plain turbidites that were uplifted by later fault movements. We were therefore faced with the question: Are these sediments primary turbidites that flowed upslope to their present position on the slope of the Tiburon Rise, or were they reworked into their present position by bottom currents? This distinction is particularly important because, if Leg 110 terrigenous beds are indeed turbidites, they represent an example of the ability of even very distal turbidity currents to deposit silt and sand significant distances upslope.

In many deep-sea sequences, distinguishing between a turbidite and a bottom-current/contourite origin can be difficult (e.g., Stow and Piper, 1982). However, in the Leg 110 case, a combination of shipboard visual core inspection, detailed post-cruise grain-size analyses, and the seismic-reflection characteris-

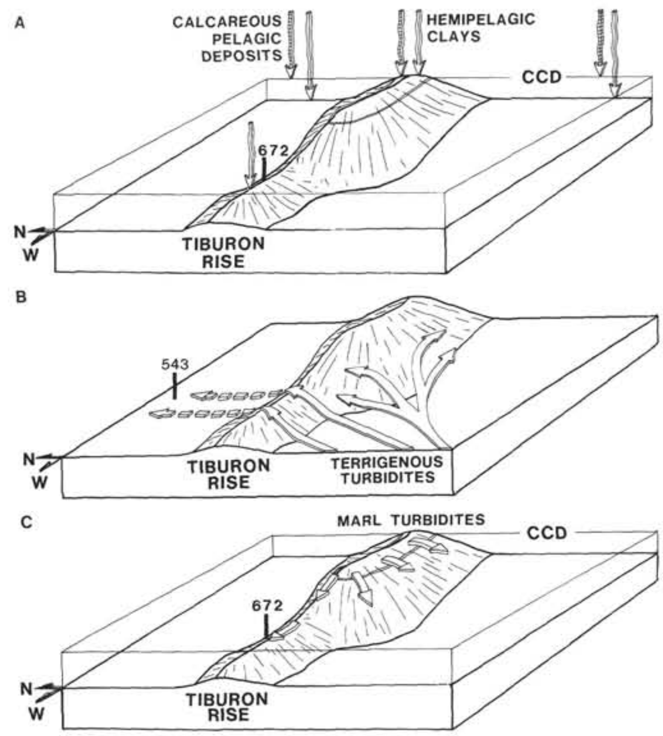

Figure 6. Schematic diagrams showing interpreted depositional patterns in the Tiburon Rise area during middle Eocene–late Oligocene time. ODP Site 672 is located on the uppermost northern slope of the western portion of the rise. (A) Deposition of hemipelagic green clay at Site 672, which was located beneath the CCD. Note interpreted location of the CCD and deposition of both hemipelagic green clay and pelagic calcareous sediment on the uppermost portions of the Tiburon Rise to the east of Site 672. (B) Deposition of South American-derived terrigenous turbidites at Site 672. Some of the turbidity currents maintained sufficient momentum to crest the lower, western portions of the Tiburon Rise (e.g., Site 672; see Dolan et al., 1989 for possible alternative explanation). These flows deposited sand and silt turbidites at the site and along the lower slopes of the southern margin of the rise (solid arrows). Broken arrows to the north of Site 672 represent continued northward flow of the clay-rich portions of the turbidity currents flowing over the lower, western portion of the rise toward DSDP Site 543. These clay-rich turbidity currents were responsible for increased middle Eocene-upper Oligocene sedimentation rates observed at Site 543. Location of Site 672 and CCD omitted for clarity. (C) One possible model for deposition of the marl turbidites and slumps. The uppermost portions of the Tiburon Rise were located above the CCD and received both pelagic calcareous sediment and hemipelagic green clay. In addition, the finest-grained portions of South American terrigenous turbidites may have deposited predominantly clay turbidites atop the rise. Periodic deposition of these clay turbidites may have caused gravitationally unstable conditions on the upper slopes of the rise and initiated downslope movement of mixed pelagic, hemipelagic, and turbiditic sediment. These mixed sediments were recovered at Site 672 as marl turbidites and slumps. Alternatively, the marl turbidites may represent deposition from the uppermost portions of the terrigenous turbidites (see text for discussion).

tics of these deposits provide strong support for a primary turbidite origin of the terrigenous beds (Fig. 6B).

The common graded bedding revealed by both shipboard visual core descriptions and by post-cruise grain-size analyses, coupled with the sharp bases to most beds, represents the most obvious evidence in support of a turbidite hypothesis. Stow and Shanmugam (1980) and Stow and Piper (1982) recognized a sequence of sedimentary structures within mud-dominated turbidites such as those recovered during Leg 110. Based on their observations, they constructed an idealized structural hierarchy consisting of nine subdivisions that encompass the Td and Te turbidite intervals of the Bouma (1962) sequence. Their model is useful for characterizing the ODP Leg 110 terrigenous beds, although we did not observe complete sequences containing all nine subdivisions. Our post-cruise grain-size analyses, coupled with shipboard visual core descriptions, indicate that the majority of the Leg 110 beds contain many of the Stow and Shanmugam (1980) T2 through P subdivisions. The common absence of the basal TO and Tl intervals is consistent with the distal nature of these turbidites, and with our interpretation that they were deposited at least several hundred meters above the abyssal plain (Fig. 6B). Common low-angle cross stratification in the terrigenous beds suggests the development of some type of bedform during deposition, possibly ripples or small dunes.

Grain-size distributions in mud and silt turbidites typically show large modes in coarse and medium silt (e.g., Kranck, 1984; Brunner and Ledbetter, 1987). In contrast, grain-size distributions in hemipelagic muds typically show large modes in fine silt (Brunner and Ledbetter, 1987). Similar patterns observed in the Leg 110 sediments add further support to our interpretation of the Leg 110 terrigenous beds as turbidites.

Multi-channel seismic reflection profile CRV 128 across the Leg 110 area also supports the turbidite hypothesis (Mascle, Moore, et al., 1988). The basal, middle- to upper Eocene portion of the anomalously coarse-grained section appears on the seismic reflection profile as a laterally continuous sheet with little lateral change in thickness (see Site 672 report, Mascle, Moore, et al., 1988). Internal reflectors are strong, parallel, and continuous. These observations are consistent with the reflection characteristics of numerous other turbidite deposits (e.g., Berg, 1982; Mitchum, 1985). In contrast, most sediment drift deposits associated with bottom-current activity are characterized by strongly mounded geometries, erosional "moats" adjacent to depositional areas, and internally complex reflector geometries associated with the migration of large-scale bedforms (e.g., Buffler et al., 1978; Faugeres et al., 1985; Kidd and Hill, 1987; Reed et al., 1987). Thus, the reflection characteristics of the Leg 110 deposits are much more consistent with a turbidite deposit.

A turbidite origin is also supported by consideration of the bottom-current velocities that would have been necessary to transport medium-grained sand up the slope of the Tiburon Rise. Most modern bottom currents associated with thermohaline deep-ocean circulation exhibit velocities on the order of 5- to 30-cm/s (e.g., MacDonald and Hollister, 1973; Flood and Hollister, 1974; Lonsdale and Malfait, 1974. Weatherly and Kelley, 1985) although locally velocities may reach as much as 70- to 75-cm/s (Emery and Ross, 1968; Kenyon and Belderson, 1973). In addition, strong currents of up to 74 cm/s have been recorded in association with short-lived benthic storms (e.g., Kerr, 1980; Tucholke et al., 1985). Although current velocities of > 20 cm/s are capable of moving low-density foraminifer sands (Southard et al., 1971), and velocites of > 30 cm/s result in development of dunes in mixed quartz-foraminifer sands (Lonsdale and Malfait, 1974), most typical bottom-current velocities (5–30 cm/s) are probably insufficient to move medium-grained terrigenous sand hundreds of meters upslope. Therefore, it seems unlikely that bottom currents would have been capable of depositing the Site 672 sands. A bottom-current origin for any of the Leg 110 terrigenous beds is therefore ruled out because the sands are an integral component of a suite of mud, silt, and sand beds which, based on textural grounds, appear to have all been deposited by the same currents.

The observations discussed above indicate that there is compelling evidence for a primary turbiditic origin for the Eocene-

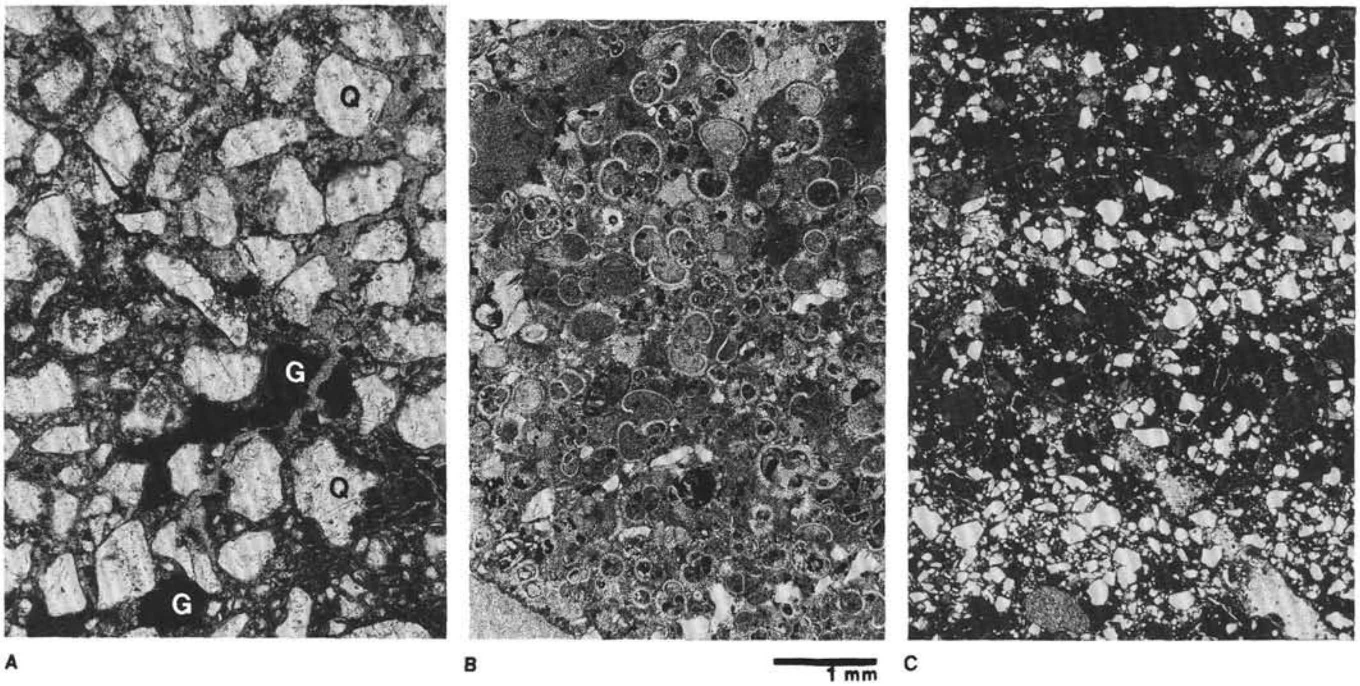

Figure 7. Photomicrographs of terrigenous beds showing the range of sediment composition. (A) Ouartz-rich fine-grained sandstone. Quartz grains [Q] are white, the dark grains [G] are composed of glauconite. Other accessory minerals in these beds include glaucophane, microcline, pyroxene, and muscovite. Sample is from ODP Hole 110-671B-74X-1, 15–19 cm. Plane light; field of view is 3.7 mm. (B) Calcareous sandstone (packstone) composed predominantly of planktonic foraminifers, many of which are filled with micrite and glauconite. Sample 110-672A-41X-CC, 18–19 cm. Plane light. (C) Mixed quartz-calcareous siltstone. Note the segregation of quartz (white) and calcareous components (dark) into distinct laminations, each approximately 0.8–1.1 mm thick. The calcareous laminations consist predominantly of planktonic foraminifers, micrite clasts, and glauconite. Sample is from Sample 110-674A-29X-1, 55–58 cm. Plane light; field of view is 3.7 mm.

Oligocene terrigenous muds, silts, and sands recovered at Site 672. These beds thus represent an exceptional example of upslope deposition of very distal turbidity currents, in this case more than 1100 km from their source (Fig. 6B).

REDEPOSITED MARLS: OBSERVATIONS

These pale green to white beds range in thickness from 1 to 45 cm and make up approximately 10% of the mid-late Tertiary section at Site 672 (Fig. 5). Shipboard smear-slide analyses indicate that these deposits consist of clay minerals and nannofossils, with a local, minor component of quartz silt.

Marl beds typically have sharp bases and either sharp or gradational tops (Fig. 10). Although many of the marl beds are internally massive, a common sequence observed in these deposits consists of: A sharp base, a horizontally laminated lower interval, a gradual upsection increase in bioturbation, and a completely bioturbated, gradational upper contact into green clay (Fig. 10). Laminations are generally horizontal with local low-angle cross stratification. Burrow types observed in the marl beds include *Planolites*, *Teichichnus*, and *Chondrites*.

In approximately 35 cases, terrigenous beds are overlain directly by redeposited marl beds; the inverse relationship occurs in only three cases. Grain-size analyses from 15 marl samples indicate a median grain size range of 5.40–7.15 phi (coarse to fine silt, Figure 9C; Appendix). Typically, the upper portions of marl beds are slightly finer grained (phi = 6.90–7.15) than overlying hemipelagic clay beds (phi = 6.60–7.00).

In addition to the redeposited marl beds, several pale green, small-scale (2 to 7 cm thick) marl slumps were recovered (Fig. 11). These typically consist of tightly folded, well-laminated sediment. The laminations are defined by alternating carbonate-rich white layers and clay-rich green layers 1- to 5-mm thick.

INTERPRETATION OF DEPOSITIONAL ENVIRONMENT

The sharp bases and gradual upward increases in bioturbation observed in many of the marl beds suggest episodic deposition, with burrowing organisms only able to penetrate the upper portions of some of the thicker beds. This accounts for the preservation of sharp lower contacts and primary basal laminations in some marl beds. These observations, coupled with grain-size analyses showing graded bedding, suggest that the marl beds are turbidites.

The common occurrence of redeposited marl beds directly over terrigenous beds suggests a genetic relationship between deposition of these two sediment types. The episodically deposited marl beds may represent either: (1) deposition from the uppermost portions of the South American terrigenous turbidity currents (Fig. 6B); or (2) turbidites composed of sediment derived from higher on the Tiburon Rise (Fig. 6C).

1. We suggest that the marl beds may represent deposition from the topmost portions of the same turbidity currents that deposited the terrigenous beds (Fig. 6B). During turbidity current transport from the South American shelf, much of the pelagic carbonate component (e.g., nannofossils, planktonic foraminifers), along with abundant clay and minor quartz silt, may have been hydraulically sorted out of the bulk of the flow, probably as a result of a lower hydraulic equivalence for these sediments than for similar-sized but denser terrigenous grains found in the lower portions of the turbidites. Individuals marl beds, (i.e., those that do not directly overlie terrigenous beds) may thus represent the most distal deposits of the South American turbidity currents, possibly derived from smaller volume flows.

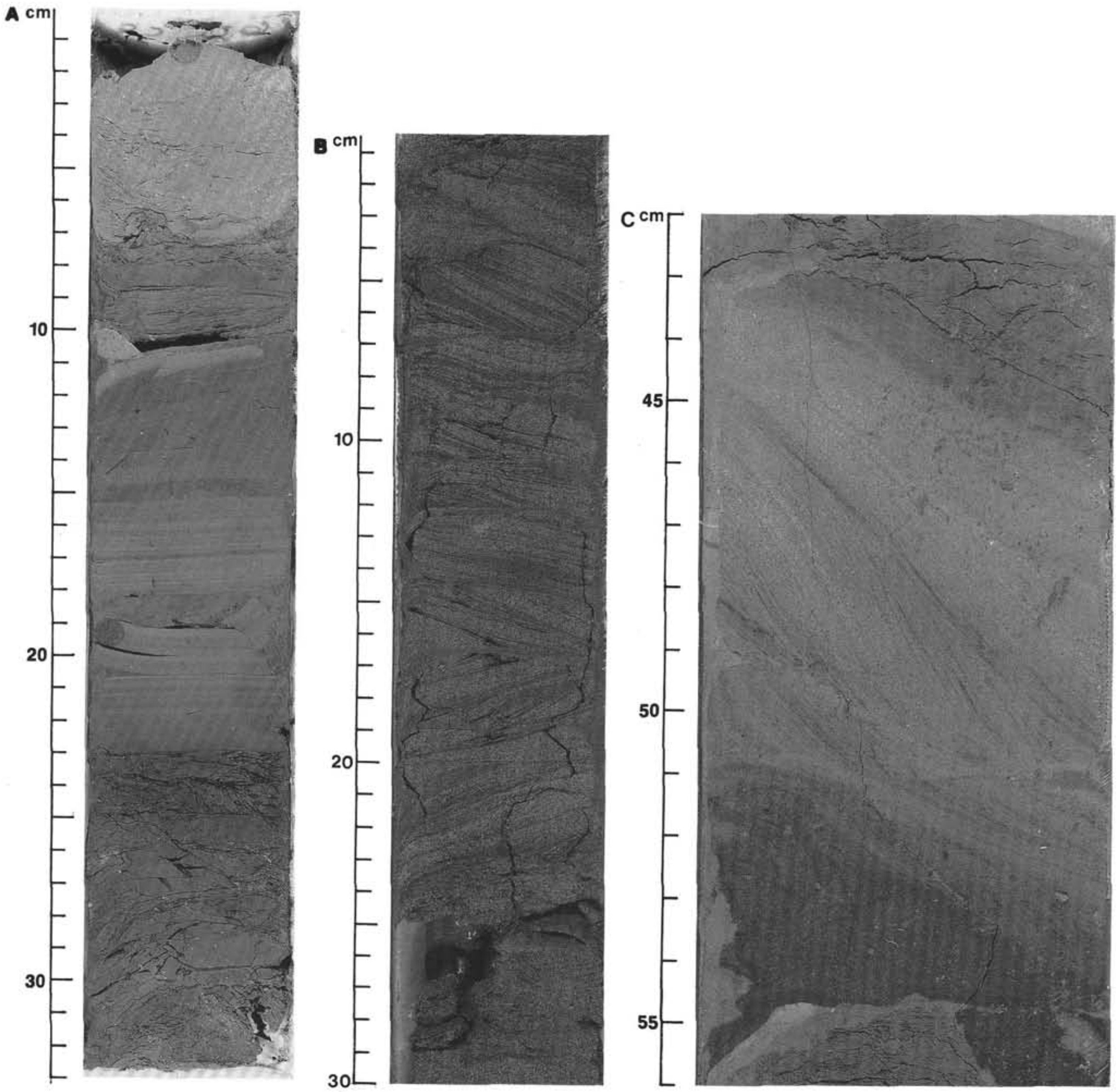

Figure 8. Core phootgraphs of sedimentary structures in terrigenous beds from ODP Leg 110 area. (A) Horizontally laminated silt bed. Note sharp base and bioturbated top of bed. Sample 110-671B-60X-CC. Scale in centimeters. (B) Low-angle to moderate-angle cross-bedding in a thick (70 cm), terrigenous fine-grained sand bed. Note that the apparent reversal in cross-lamination dip direction at 16.5 cm is a drilling artifact caused by differential rotation between adjacent "drill biscuits." Section 110-672A-48X-2, 0–30 cm. (C) A rare example of high-angle cross-bedding in a calcareous fine-grained sand bed. Section 110-672A-40X-5, 42–56 cm. (D) Probable example of multiple sediment pulses within a single terrigenous interval. Note the abrupt up-core changes in sedimentary structures, including an interval of mesoscopic graded bedding from 89.2–88.1 cm (left side of core). Scale is in centimeters. Section 110-671B-61-4. (E) Thin, non-graded bed of fine quartz sand located within an interval of featureless green clay. Section 110-671B-74X-1.

2. Alternatively, the marls may have been deposited by turbidity currents derived from higher on the Tiburon Rise (Fig. 6C). We speculate that the finest-grained portions of the terrigenous turbidites may have been partially deposited along the upper slopes of the rise (Figure 6B). Because the uppermost portions of the Tiburon Rise were probably above the CCD (Fig. 6A), deposition of very fine-grained turbidites may have led to gravitationally unstable, mixed terrigenous/pelagic-carbonate deposits on the upper slopes of the rise. We hypothesize that these deposits slumped off the rise and were deposited as marl turbidites and slumps on the lower slopes of the rise, where we encountered them at Site 672. The small-scale marl slumps in the middle Eocene-upper Oligocene interval consist of the same pale green clay-nannofossil marl as the marl turbidites, supporting the possibility that mixed clay-pelagic carbonate deposits occurred upslope from Site 672.

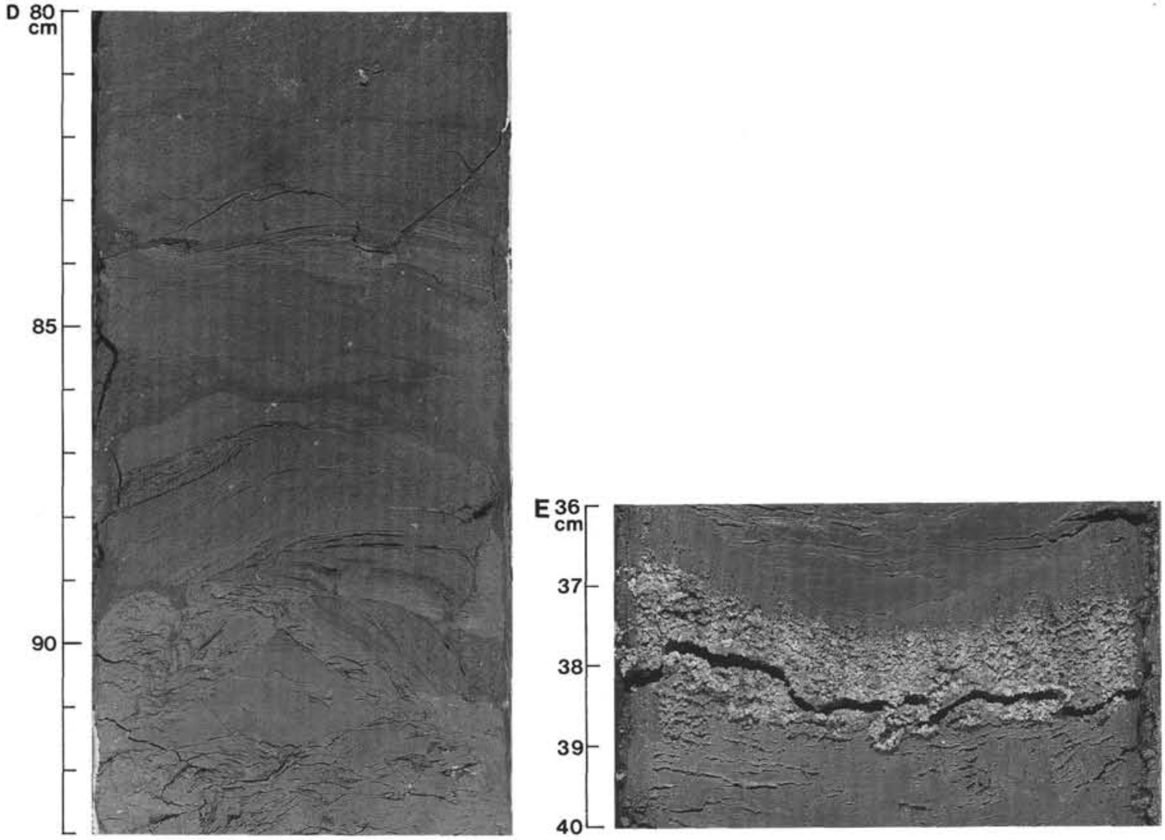

Figure 8 (continued).

COMPARISON OF SITE 672 WITH NEARBY DSDP SITES 543 AND 27

The pronounced along-strike bathymetric relief of the Tiburon Rise suggests that turbidite depositional rates varied widely along the rise. Site 672 is located along the nose of the Tiburon Rise, on the uppermost northern slope (Figures 2, 4). We suggest that the terrigenous deposits recovered at this site represent deposition of silt- and sand-sized sediment carried by the turbidity currents as they slowed during their climb up, and locally over, the rise (Figure 6B; for more complete discussion see Dolan et al., 1989).

The absence of similar coarse-grained terrigenous turbidites of middle Eocene–upper Oligocene age in DSDP Hole 543 to the north of the Tiburon Rise (Fig. 2) supports our hypothesis that the rise acted as a barrier to the northward transport of South American-derived turbidity currents during mid to late Tertiary time. Site 543 is located just to the north of the Tiburon Rise, only 19 km north of Site 672 (Fig. 2). Despite this proximity, middle Eocene-upper Oligocene deposits at Site 543 consist exclusively of clay and pelagic clay (see Site 543 site report; Moore, Biju-Duval, et al., 1984). However, sedimentation rates at Site 543 do increase in the middle Eocene–upper Oligocene section (J. C. Moore, pers. commun., 1987). We suggest that these increased mid-late Tertiary sedimentation rates observed in Hole 543 reflect deposition of the predominantly clay-sized component of the South American turbidity currents. Only the very fine-grained, clay-rich suspended load of the uppermost portions of these turbidity currents was able to spill over the Tiburon Rise and reach Site 543 (Fig. 6B).

DSDP Site 27, which is located along the southern flank of the Barracuda Ridge approximately 150 km ENE of Site 672 (Fig. 3), contains common, upper middle Eocene, very thin-bedded (1- to 5-mm) marl turbidites that may correlate with similar beds described from Site 672. In addition, one thin probable upper Oligocene marl turbidite was recovered at Site 27. This bed may correlate with upper Oligocene marl and terrigenous turbidites recovered at Site 672. No terrigenous turbidites were identified at Site 27, although it is important to note that this site was only spot cored, in contrast to Sites 543 and 672, which were continuously cored. The Site 27 marls are interbedded with green clays similar to the hemipelagic "background" clays recovered at Site 672.

By analogy with Site 672, we suggest that the Site 27 marls represent either: (1) very distal deposition of the uppermost portions of South American-derived turbidites, which either flowed northward over, or around, the bathymetric barrier imposed by the Tiburon Rise and its associated bathymetric trough (Fig. 3), or (2) turbidites composed of mixed hemipelagic green clay and pelagic carbonate that was originally deposited along the uppermost slopes of the Barracuda Ridge.

ESTIMATES OF PALEOGENE BATHYMETRIC RELIEF AND SURFACE SLOPE OF THE TIBURON RISE AND SITE 672

The paleobathymetry of the area to the southwest of the Tiburon Rise is potentially critical in terms of understanding paleo-sediment dispersal patterns for the Eocene-Oligocene deposits discussed in this paper. Unfortunately, this area has been completely over-ridden during the past 25 m.y. by the eastward-moving Lesser Antilles island arc and accretionary prism (Fig. 1). Consequently, we cannot reconstruct the mid-late Tertiary paleobathymery of the area. However, we can provide minimum and maximum estimates of relief along the Tiburon Rise during

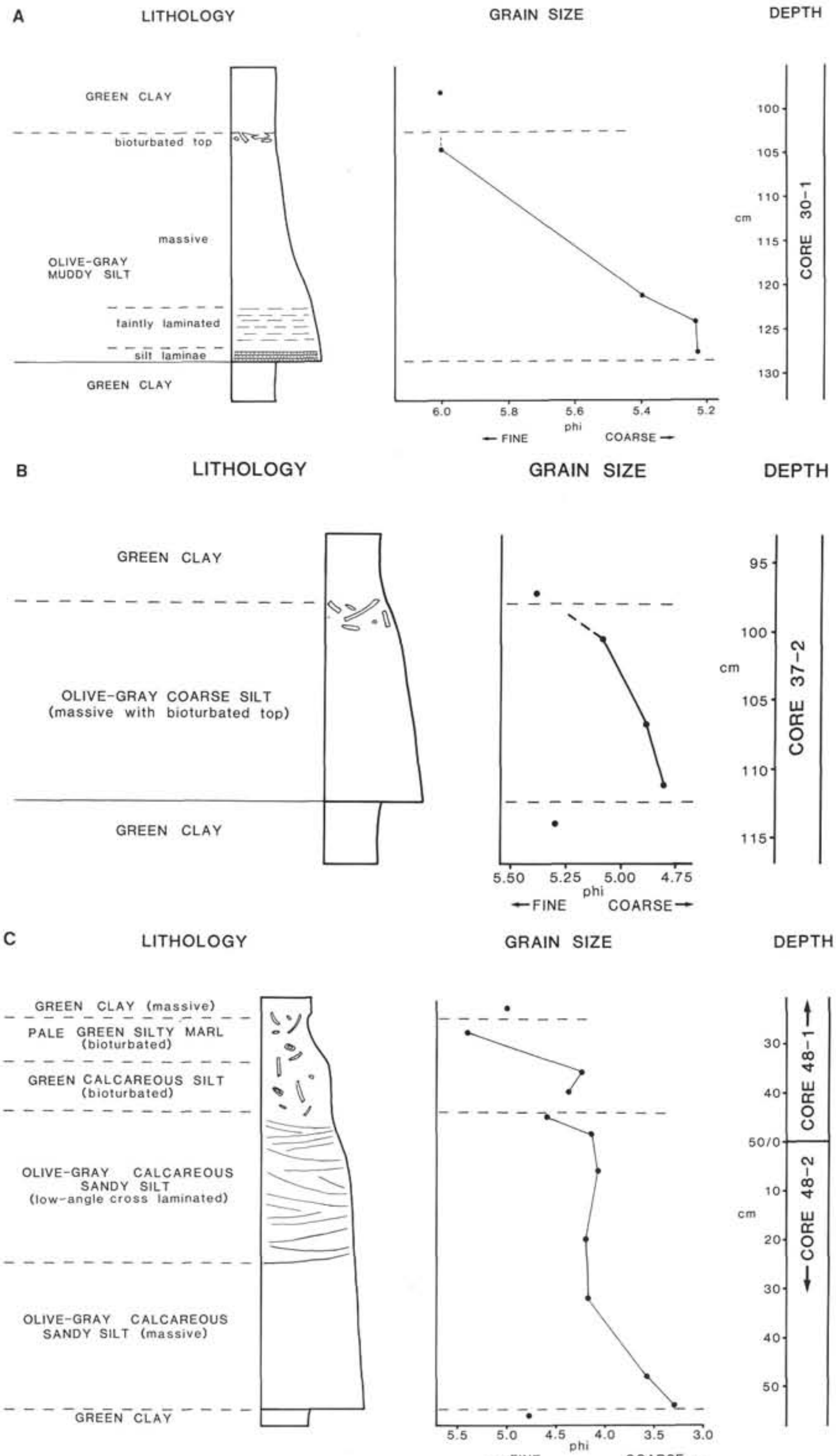

Figure 9. Examples of grain-size analyses of ODP Leg 110 sediments. (A) Graded bedding in a terrigenous silt and mud bed. Note that in addition to positive grading, this bed exhibits a sharp base, basal silt laminations, a massive upper portion, and a bioturbated top into green clay. These features are typical of many of the terrigenous beds. Section 110-672A-30X-1. (B) Terrigenous silt bed exhibiting sharp base and graded bedding. Note that the apparent, relatively coarse grain size shown for the enclosing clay beds (phi = 5.3–5.4) is an artifact of the aperture size used in this grain-size analysis. See Appendix for discussion. Section 110-672A-37X-2. (C) Graded terrigenous sandy-silt bed overlain by a graded marl bed. Note the grain-size increase at the terrigenous bed/marl bed contact. The upper portion of this terrigenous bed is shown in Figure 9B. As in (B) above, the sampling aperture used in these grain-size analyses results in artificially coarse grain sizes for the the finer-grained portions of these beds (see Appendix). Sections 110-672A-48X-1 and -2.

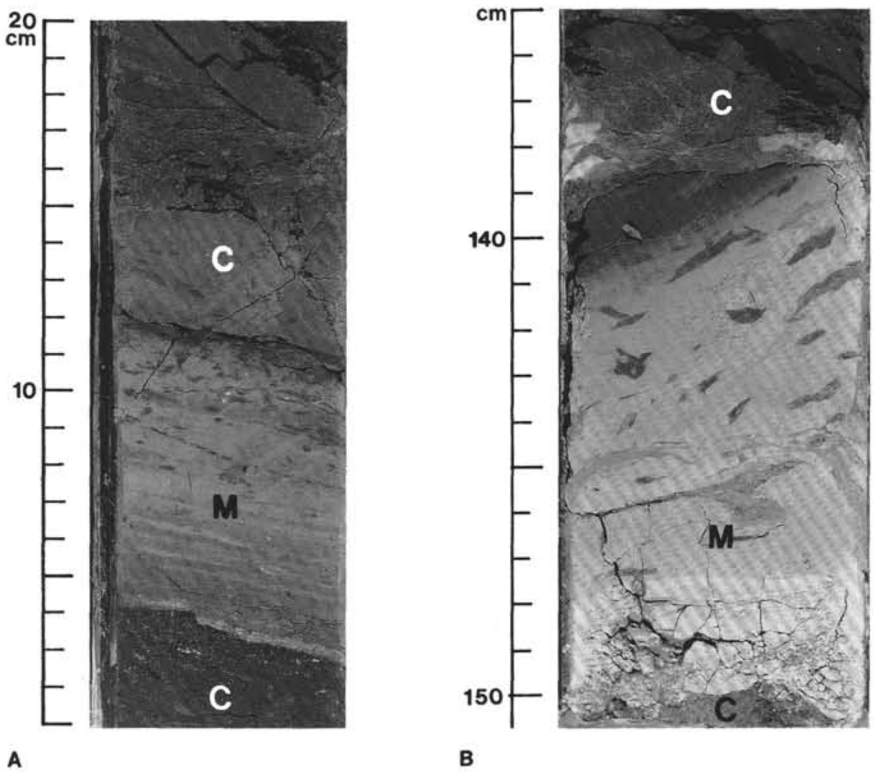

Figure 10. Core photographs of marl beds from the Leg 110 area. (A) Marl turbidite [M] exhibiting well-developed sequence of sedimentary structures typical of these beds. Note the sharp base, basal laminated interval, increasing bioturbation upsection, and the gradational top of the bed into green clay [C]. This example is from an overturned interval in Section 110- 674A-29X-CC. Scale is in centimeters. (B) Another example of a well-developed marl turbidite. Note the laminated basal portion of the marl bed [M] and the highly gradational, bioturbated top of the bed. The overlying and underlying beds consist of green clay [C]. Section 672A-40X-4.

this time period based on depth-to-basement maps, seismic reflection profiles, and the knowledge that most vertical fault movements had ceased by late Eocene time (see discussion above).

Analysis of the seismic reflection profile across the southeastern Tiburon Rise (Peter and Westbrook, 1976; their Fig. 15) shows that relief along the southern side of the rise has decreased steadily with time as sediment both onlapped and draped the rise. Thus, present surface relief along the southern margin represents the *minimum* amount of relief that has existed throughout the history of the rise. Site 672 presently lies at 4975 m water depth on the western nose of the Tiburon Rise, slightly north of the rise crest (Fig. 2). The site is approximately 600 m above the abyssal plain to the north (Fig. 3). The present slope of the northern margin of the Tiburon Rise dips at 1.8° to 2.6°, whereas the southern slopes dip more steeply (4.0°–5.0°; Fig. 3). These steep southern slopes are probably related to impingement of the accretionary prism in this area.

Given the ridge-and-trough bathymetry of the surrounding area, it is unlikely that the seafloor to the south of the Tiburon Rise was any shallower than the abyssal plain to the north of the rise (prior to eastward encroachment of the accretionary prism into the area). Thus, the present 600-m-relief along the northern margin of the rise probably represents the *minimum* amount of relief along the southern margin of the rise since cessation of most normal fault movements in late Eocene time.

We can approximate one other datum for the area to the southwest of the Tiburon Rise, depth to basement, which represents an absolute *maximum* amount of relief along the rise. These estimates are based on a combination of the depth-to-basement maps from the Tiburon Rise area and the regionally consistent, pronounced WNW–ESE trend of basement features in the area. However, the estimates ignore sediment infilling of basement lows. Because much of the infilling of the basement lows may have been early (i. e., Late Cretaceous-Paleocene), the depth-to-basment estimates probably greatly overestimate the Eocene–Oligocene relief between Site 672 and the adjacent seafloor. Note also that these estimates have not been corrected for sediment compaction effects, which would also tend to increase apparent basement relief.

Depth-to-basement maps indicate that the paleo-ridgecrest of the Tiburon Rise was located in approximately the same place as the present crestline (Fig. 3; Westbrook et al., 1966). Furthermore, they show that the rise has had basically the same morphology since at least late Eocene time (and probably since Late Cretaceous time; Fig. 3). Basement slopes of the northern margin of the rise dip from 1.8° to 4.0°, approximately the same angle as the present surface slopes, and total basement relief here is approximately 1.5- to 3.1 km (Fig. 3). In contrast, basement maps indicate that the southeastern margin of the rise has much higher basement relief and basement slopes. In this area, total relief from the ridge crest to the base of the deep trough along the southern margin of the rise ranges from 1.8 km to at least 4.5 km, with surface slopes of 3.0°–6.8°. The measurements for these latter calculations are taken for slopes east of the accretionary prism deformation front only (i.e., east of 57°35′ W), and represent minimum values, because the trough apparently continues to deepen toward the west beneath the accretionary prism, whereas the rise shallows toward the west (Fig. 3).

We can reconstruct two approximate "end-member" depth-to-basement scenarios for the region to the southwest of the Ti-

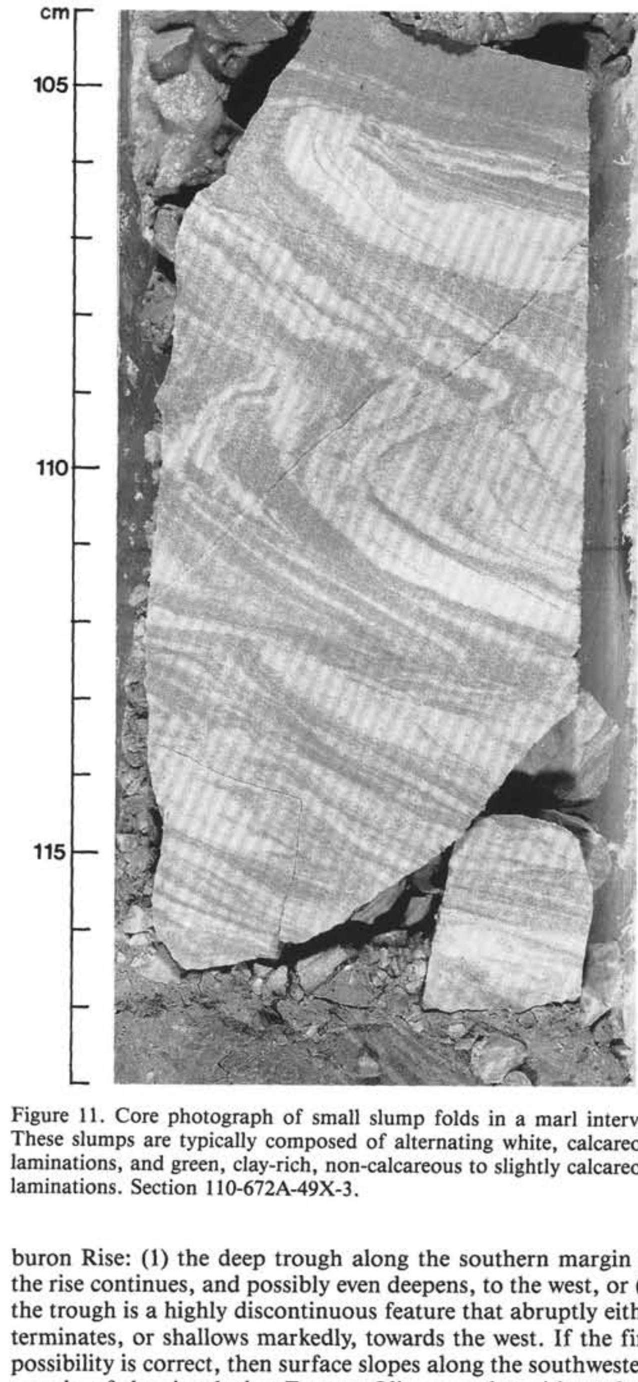

Figure 11. Core photograph of small slump folds in a marl interval. These slumps are typically composed of alternating white, calcareous laminations, and green, clay-rich, non-calcareous to slightly calcareous laminations. Section 110-672A-49X-3.

buron Rise: (1) the deep trough along the southern margin of the rise continues, and possibly even deepens, to the west, or (2) the trough is a highly discontinuous feature that abruptly either terminates, or shallows markedly, towards the west. If the first possibility is correct, then surface slopes along the southwestern margin of the rise during Eocene-Oligocene deposition of the Site 672 terrigenous turbidites may have been quite high. In this scenario, maximum basement relief would be at least 4.5 km, and possibly higher. Because the basement at Site 672 is located approximately 1.2 km below the crest of the ridge, basement relief between the drill site and the seafloor to the south may therefore have been as much as 3.3 km. By analogy to the southeastern margin of the rise, surface slopes may have been 7° or steeper. If, on the other hand, the trough terminates toward the west, total surface relief along the southwestern margin of the rise would have been approximately 2 km (using a conservatively estimated "average abyssal plain" depth for the region of 6.5 km; see Fig. 3). Total basement relief between Site 672 and the adjacent seafloor may therefore have been as little as 800 m. In this second scenario, basement slopes of the rise might have been as shallow as approximately 1.5°. We cannot presently choose between these two possibilities. However, the apparent westward deepening of the trough beneath the toe of the accretionary prism suggests that the first scenario may be the more likely one.

UPSLOPE DEPOSITION OF TURBIDITES

Experimental evidence and theoretical models indicate that turbidity currents can flow significant distances upslope, particularly if they are large, unconfined flows (e.g., Muck and Underwood, in press). Recent experiments on saline fluid density currents indicate that the thickness of a turbidity current must be greater than approximately 60% of the height of the bathymetric obstruction to promote transfer of any material over the crest of the barrier (Muck and Underwood, in press). For example, if the Tiburon Rise crest-to-abyssal plain elevation was 800 m during deposition of a given terrigenous bed, then the thickness of the turbidity current that deposited that bed must have been at least 480 m. These results suggest that the turbidites recovered at Site 672 were deposited by very high-volume or high-concentration flows, considering that Site 672 was located more than 1100 km from the point of turbidity current initiation.

Upslope flow of turbidity currents has been reported from a number of environments (e.g., Van Andel and Komar, 1969; Damuth and Embley, 1979; Damuth, 1979; Cita et al., 1984; Underwood, 1987). In one example from the Aleutian trench, sand-rich turbidity currents derived from the Aleutian arc flowed down the inner trench slope, into the trench, and then continued up the opposite, seaward trench slope. Thin sand turbidites here have been recovered on the outer trench slope as much as 1000 m above the trench floor (Underwood, 1987). Similarly, in the Ceara Rise off northeastern South America, piston cores and 3.5-kHz echograms indicate that thin turbidites have been deposited as much as 400 m above the Amazon cone/Ceara Rise boundary (Damuth and Embley, 1979). These examples, coupled with the ODP Tiburon Rise example discussed here, suggest that upslope flow of turbidity currents may be a more common process than has been previously thought.

Although the term "upslope flow" has generally been used to describe these deposits, turbidite deposition on the slope of a bathymetric barrier may actually result from a combination of two processes: (1) True upslope flow. When a turbidity current encounters an obstruction, the center of mass of the current will move upwards, facilitating some genuine upslope flow that may result in upslope deposition (Muck and Underwood, in press). (2) Alternatively, upslope turbidite deposition may result simply as a consequence of the upper portions of thick turbidity currents intersecting the slope (e.g., Damuth, 1979; Muck and Underwood, in press). Separating these two mechanisms may prove to be difficult in the absence of definitive evidence of turbidity current thickness.

True upslope flow may occur when a hydraulic jump experienced by the turbidity current (i.e., transition from supercritical to subcritical flow) is delayed until the current has at least partially surmounted the bathymetric barrier (Muck and Underwood, in press). However, in the case of the distal Leg 110 turbidity currents, it seems highly unlikely that supercritical flow conditions might be maintained over such long transport distances (>1100 km). Consequently, we feel that this is not a realistic mechanism for deposition of the Leg 110 deposits. However, even if flow conditions in the turbidity currents were subcritical, some true upslope flow may have occurred as momentum carried the currents partially up the Tiburon Rise.

Alternatively, much of the sediment deposited on the Tiburon Rise may simply represent deposition from the upper portions of very thick turbidity currents that intersected the slope. Deposition from very thick (600- to 900-m) turbidity currents has been reported from several deep submarine channels (e.g., Embley and Langseth, 1977; Normark et al., 1979) and from the seaward wall of the Manila Trench (Damuth, 1979). However, it remains unclear whether or not turbidity currents this thick also occur in unchannelized, distal settings as well. If the Leg 110 turbidity currents were channelized, confined flows over much of their transport to the Tiburon Rise area, this type of deposition may offer a reasonable explanation for deposition of the Eocene–Oligocene terrigeous turbidites. We can only speculate on this point, because the most probable paleo-sediment dispersal route from South America to the Tiburon Rise lies beneath the Lesser Antilles accretionary prism (Fig. 1; Beck et al., this volume).

SITE 672 TERRIGENOUS BEDS

At ODP Site 672, the total number of terrigenous beds (at least 258) divided by the overall time period of terrigenous deposition (14–16 m.y.) yields a recurrence interval of approximately 60 to 65 k.y. (based on a recovery rate of 72%). The triggering mechanism for initiation of the turbidity currents is not known, but may have been earthquakes in the tectonically active South American borderland (Beck et al., this volume).

Paleogeographic reconstructions of northern South America during Paleogene time suggest that the up-section decrease in grain size observed at Site 672 may have been partially controlled by tectonic events in northern Venezuela (Beck et al., this volume). During Eocene time, the northern portion of South America was dominated by a large, northeast-opening embayment characterized by widespread deposition of glauconitic sands, known as the Caratas Formation (Beck et al., this volume). These sands probably acted as the major source for the common, pale green, glauconitic-foraminifer sandstones recovered at Site 672. At approximately the Eocene-Oligocene boundary, the onset of major right-lateral strike-slip faulting in northern Venezuela closed this embayment, shutting off supply of these sands. This event is reflected in the uphole decrease in glauconitic-foraminifer sand at approximately the Eocene-Oligocene boundary at Site 672 (Fig. 5).

Minor uplift of the Tiburon Rise during the late Eocene probably acted as an additional cause for the up-section decrease in terrigenous turbidite grain size at Site 672. As discussed above, seismic-reflection profiles indicate that most normal fault displacement along the margins of the Tiburon Rise occurred prior to Eocene time. However, minor differential uplift of the rise continued until at least the late Eocene. This observation indicates that the rise was probably a slightly less pronounced bathymetric barrier to northward turbidity current flow during deposition of the Eocene portion of the coarse-grained sediments, allowing deposition of fine- and medium-grained sand at Site 672. During late Eocene time, minor fault movements apparently slightly increased the height of the rise. This increased height probably inhibited upslope flow of the coarsest-grained, basal portions of the terrigenous turbidity currents, and may account for the deposition of mainly silt and mud turbidites at Site 672 during Oligocene time.

RELATIONSHIP TO EUSTATIC SEA-LEVEL CHANGES

Sedimentation rates calculated for the middle Eocene-upper Oligocene interval at Site 672 reveal two distinct pulses of increased sedimentation rates that correlate with increased percentages of terrigenous beds (Figs 6, 13). These pulses occurred during late middle Eocene time (upper part of nannofossil Zones CP14A and CP14B) and late early Oligocene time (nannofossil Zone CP16). Comparison of the ages of these two sediment pulses with eustatic sea-level curves indicates that they correlate approximately with eustatic sea-level high stands (Fig. 12; Haq et al., 1987). This is exactly the opposite relationship predicted by most models of deep-sea terrigenous sedimentation (Vail et al., 1977; Shanmugam and Moiola, 1982; Haq et al., 1987). Because similar occurrences of anomalously coarse-grained terrigenous sediment do not occur in the Leg 110 area in association with later, similar Neogene sea-level high stands, deposition of the coarse-grained Leg 110 sediments was apparently not directly related to eustatic sea-level changes. Rather, as discussed above, deposition probably resulted from pulses of increased sediment supply from the South American shelf, which were controlled by tectonic movements along the northern South American borderland (see Beck et al., this volume). This demonstrates that along active margins (e.g., northern South America), tectonically induced increases in sediment supply can completely overwhelm any eustatic signal.

REGIONAL SIGNIFICANCE

The occurrence of extensive terrigenous deep-sea sedimentary rocks of middle Tertiary age in the Tiburon Rise area and on the island of Barbados invites comparison of these two deposits (Fig. 1). The Scotland Group of Barbados consists of a thick sequence of quartzose turbiditic sandstones (Velbel, 1980;, Speed and Larue, 1982; Pudsey and Reading, 1982; Kaspar and Larue, 1986). Accessory minerals in these quartz wackes include glauconite, microcline, zircon, and glaucophane, in addition to foraminifers and other shell debris (Velbel, 1980; Pudsey and Reading, 1982; Kaspar and Larue, 1986); this is essentially the same accessory mineral assemblage observed in the Leg 110 quartzose silts and sands.

Biostratigraphic studies of the Scotland Group have suggested that these deposits are predominantly lower and middle Eocene in age (Fig. 13; Speed and Larue, 1982). However, a recent fission-track study of zircons from the Scotland Group indicates ages as young as late Oligocene, suggesting that many microfossils in the Scotland Group may be reworked (Fig. 13; Baldwin et al., 1986). This study indicates that the Scotland Group beds are approximately the same age as the Leg 110 terrigenous turbidites (Fig. 13).

Despite the similarity in ages of the Leg 110 and Scotland Group deposits, compositional differences suggest that the two deposits had markedly different (but overlapping) sediment source areas. Although the quartzose silts and sands of both areas are remarkably similar in composition, these deposits dominate the Scotland Group, whereas they are volumetrically minor in the Leg 110 area. The Leg 110 sediments contain much more glauconite and calcareous detritus, particularly planktonic foraminifers and micrite clasts.

Kaspar and Larue (1986) and Baldwin et al. (1986) suggest that the Scotland Group sandstones were derived predominantly from the Guyana Shield and the Caribbean Mountain System. In contrast, although the volumetrically subordinate quartzose sediments of the Leg 110 area were probably derived from similar sources, the bulk of the Leg 110 terrigenous sediment was probably derived from the South American shelf (Beck et al., this volume).

The Lesser Antilles accretionary prism, of which Barbados is a part, has been migrating toward the east since at least Eocene time, although the exact timing and amount of migration is a matter of debate (Speed, 1985; Pindell and Barrett, in press). In contrast, the Tiburon Rise, as part of the South America/South Atlantic Plate, has not migrated with respect to South America. This observation suggests that the Leg 110 sediments may have been derived from a more easterly source terrane than the Scotland Group sediments.

CONCLUSIONS

1. A 220-m-thick, laterally continuous unit in the Tiburon Rise area consists of three sediment types: (A) terrigenous mud, silt, and sand turbidites derived from South America, (B) marl

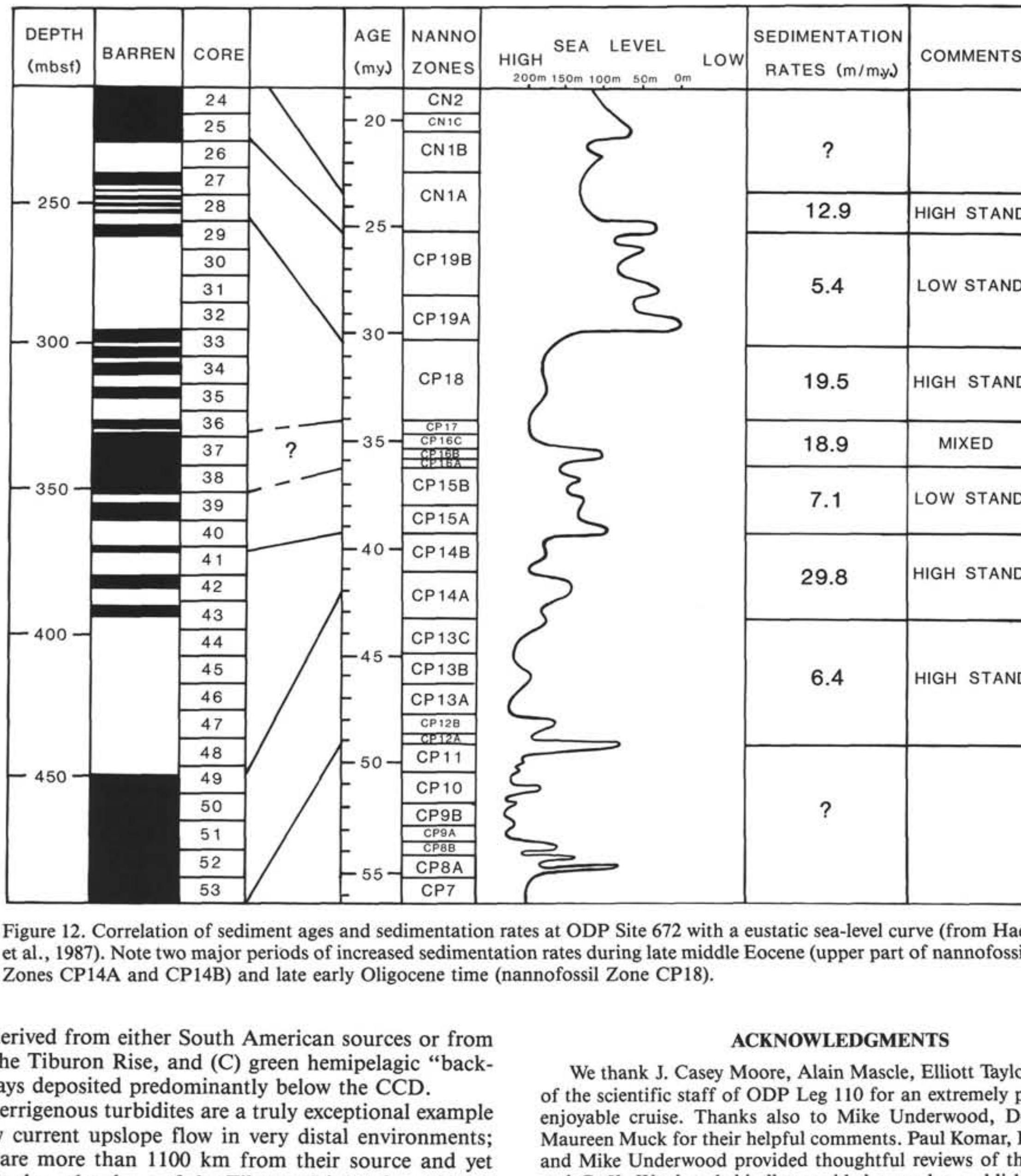

Figure 12. Correlation of sediment ages and sedimentation rates at ODP Site 672 with a eustatic sea-level curve (from Haq et al., 1987). Note two major periods of increased sedimentation rates during late middle Eocene (upper part of nannofossil Zones CP14A and CP14B) and late early Oligocene time (nannofossil Zone CP18).

turbidites derived from either South American sources or from higher on the Tiburon Rise, and (C) green hemipelagic "background" clays deposited predominantly below the CCD.

2. The terrigenous turbidites are a truly exceptional example of turbidity current upslope flow in very distal environments; these beds are more than 1100 km from their source and yet were deposited on the slope of the Tiburon Rise at least 800 m above the surrounding abyssal plain.

3. Sedimentation rates for the mid-late Tertiary section reveal two distinct pulses of increased sedimentation that correlate with increased percentages of terrigenous beds. These pulses occurred during late middle Eocene and late early Oligocene time. We propose that the sediment pulses observed at Site 672 are related to periods of increased tectonic activity in northern South America that resulted in increased terrigenous sediment supply.

4. The quartzose Scotland Group turbidites of Barbados are approximately the same age as the terrigenous muds, silts, and sands recovered at Site 672, suggesting that deposition of both units may have been related to the tectonic pulses proposed above. However, although the quartz-rich beds at Site 672 overlap compositionally with the Scotland Group sandstones, the majority of the Leg 110 terrigenous sediments contain much more abundant shelf-derived carbonate detritus, suggesting different source areas for the two deposits.

ACKNOWLEDGMENTS

We thank J. Casey Moore, Alain Mascle, Elliott Taylor, and the rest of the scientific staff of ODP Leg 110 for an extremely productive and enjoyable cruise. Thanks also to Mike Underwood, Don Reed, and Maureen Muck for their helpful comments. Paul Komar, Dallas Abbott, and Mike Underwood provided thoughtful reviews of the manuscript, and G. K. Westbrook kindly provided several unpublished seismic-reflection profiles. Financial support for post-cruise research was provided by a JOIDES grant administered by the Texas A&M Research Foundation. Grain-size analyses were carried out at the Moss Landing Marine Lab under the supervision of Mike Ledbetter.

REFERENCES

Baldwin, S., Harrison, T., and Burke, K., 1986. Fission track evidence for the source of accreted sandstones, Barbados. *Tectonics*, 5:457–468.

Blaeser, C. R., and Ledbetter, M., 1982. Deep-sea bottom currents differentiated from texture of underlying sediment. *J. Sediment. Petrol.*, 52: 755–768.

Bouma, A. H., 1962. *Sedimentology of Some Flysch Deposits*: Amsterdam (Elsevier).

Bourgois, J., von Huene, R., Pautot, G., and Huchon, P., 1988. *Jean Charcot* Seabeam survey along ODP Leg 112 northern transect. *In* Suess, E., von Huene, R., et al., *Proc, ODP, Init. Repts.*, 112: College Station, TX (Ocean Drilling Program), 131–137.

Brunner, C. A., and Ledbetter, M. T., 1987. Sedimentological and micropaleotological detection of turbidite muds in hemipelagic sequences: An example from the late Pleistocene levee of Monterey Fan, central California continental margin. *Mar. Micropaleontol.*, 12: 223-239.

Buffler, R., Shipley, T., and Watkins, J., 1978. Blake Continental Margin seismic section. *AAPG Seismic Section No. 2.* AAPG Seismic Line Series.

Cita, M., Beghi, C., Camerlenghi, A., Kastens, K., McCoy, F., Nosetto, A., Parisi, E., Scolari, F., and Tomadin, L., 1984. Turbidites and megaturbidites from the Herodotus abyssal plain (eastern Mediterranean) unrelated to seismic events. *Mar. Geol.*, 55:79-101.

Damuth, J. E., 1979. Migrating sediment waves created by turbidity currents in the northern South China Sea. *Geology*, 7:520-523.

Damuth, J. E., and Embley, R. W., 1979. Upslope flow of turbidity currents on the northwest flank of the Ceara Rise: Western equatorial Atlantic. *Sedimentology*, 26:626-634.

Dolan, J. F., Beck, C., and Ogawa, Y., 1989. Upslope deposition of extremely distal turbidites: An example from the Tiburon Rise, west-central Atlantic. *Geology*, 17:990-994.

Embley, R. W., and Langseth, M. G., 1977. Sedimentation processes on the continental rise of northeastern South America. *Mar. Geol.*, 25: 279-297.

Emery, K., and Ross, D., 1968. Topography and sediments of a small area of the continental slope south of Martha's Vineyard. *Deep-Sea Res.*, 15:415-422.

Faugeres, J. C., Gonther, E., and Poutiers, J., 1985. Facies and sediment dynamics in Charlie-Gibbs Fracture Zone during the late Quaternary. *Mar. Geol.*, 52:101-119.

Flood, R. D., and Hollister, C. D., 1974. Current-controlled topography on the continental margin off the eastern United States. *In* Burk, C., and Drake, C. (Eds.), *The Geology of Continental Margins*: New York (Springer-Verlag Press), 197-205.

Haq, B., Hardenbol, J., and Vail, P., 1967. Chronology of fluctuating sea levels since the Triassic. *Science*, 235:1156-1167.

Hilde, T., Warsi, W., and Searle, R., 1985. GLORIA long-range, side-scan sonograph mosaic. *In* Hussong, D., Dang, S., Kulm, L., Couch, R., and Hilde, T. (Eds.), *Atlas 9, Peru-Chile Trench off Peru. Ocean Margin Drilling Program Regional Atlas Series*, Woods Hole, MA (Marine Science International).

Kaspar, D. C., and Larue, D. K., 1986. Paleogeographic and tectonic implications of quartzose sandstones of Barbados. *Tectonics*, 5:837-854.

Kenyon, N., and Belderson, R., 1973. Bedforms of the Mediterranean undercurrent observed with side-scan sonar. *Sediment. Geol.*, 9:77-99.

Kerr, R. A., 1980. A new kind of storm beneath the sea. *Science*, 206: 484-467.

Kidd, R. B., and Hill, P. R., 1987. Sedimentation on Feni and Gardar sediment drifts. *In* Ruddiman, W. F., and Kidd, R. B. (Eds.), *Init. Repts. DSDP*, 94, Pt. 2: Washington (U.S. Govt. Printing Office), 1217-1244.

Kranck, K., 1984. Grain-size characteristics of turbidites. *In* Stow, D.A.V., and Piper, D.J.W. (Eds.), *Fine-Grained Sediments: Deep-Water Processes and Facies*: (Oxford) Blackwell Scientific Publishers, 63-92.

Lonsdale, P., and Malfait, B., 1974. Abyssal dunes of foraminiferal sands on the Carnegie Ridge. *Geol. Soc. Am. Bull.*, 65:1697-1712.

MacDonald and Hollister, 1973. Near-bottom thermocline in the Samoan Passage, west equitorial Pacific. *Nature*, 243:461-462.

Mascle, A., Moore, J. C., et al., 1988. *Proc. ODP, Init. Repts.*, 110: College Station, TX (Ocean Drilling Program).

Mauffret, A., Westbrook, G. K., Truchan, M., and Ladd, J., 1984. The relief of the oceanic basement and the structure of the front of the accretionary complex in the region of sites 541, 542, and 543. *In* Biju-Duval, B., Moore, J. C., et al., *Init. Repts. DSDP*, 78A: Washington, D.C. (U.S. Govt. Printing Office), 49-62.

Mitchum, R. M., Jr., 1985. Seismic stratigraphic expression of submarine fans. *In* Berg, 0. R., and Woolverton, D. G. (Eds.), *Seismic Stratigraphy II: An Integrated Approach to Hydrocarbon Exploration. AAPG Mem.*, 39:117-136.

Moore, J. C., Biju-Duval, B., Bergen, J. A., Blackington, G., Claypool, G. E., Cowan, D. S., Davis, D., Guerra, R. T., Hemleben, C., Marlow, M., Pudsey, C., Renz, G. W., Tardy, M., Wilson, D. S., and Wright, A., 1984. Site Report, DSDP Site 543: Oceanic reference site east of the Barbados ridge complex. *In* Moore, J. C., and Biju-Duval, B., et al., *Init. Repts. DSDP*, 78A: Washington, D. C. (U. S. Govt. Printing Office), 227-296.

Muck, M., and Underwood, M. B., in press. Upslope flow of turbidity currents: A comparison between empirical data, theory, and laboratory models. *Geology*.

Normark, W. R., Hess, G. R., Stow, D. A., and Bowen, A. J., 1980. Sediment waves on the Monterey Fan levee: A preliminary physical interpretation. *Mar. Geol.*, 37:1-18.

Peter, G., and Westbrook, G. K., 1976. Tectonics of the southwestern North Atlantic and Barbados Ridge Complex. *AAPG Bull.*, 60: 1076-1106.

Pindell, J., and Barrett, S. F., in press. Geological evolution of the Caribbean region: A plate-tectonic perspective. *In* Case, J. E., and Dengo, G. (Eds.), *Caribbean Region. Decade of North American Geology*: 11, Boulder (Geological Society of America).

Pudsey, C. J., and Reading, H. G., 1982. Sedimentology and structure of the Scotland Group, Barbados. *In* Leggett, J. K. (Ed.), *Trench-forearc geology: Sedimentation and tectonics on modern and ancient active plate margins*. Geol. Soc. London, Spec. Publ., 10: Oxford (Blackwell Scientific Press), 291-306.

Reed, D., Meyer, A., Silver, E., and Prasetyo, H., 1987. Contourite sedimentation in an intraoceanic forearc system: Eastern Sunda Arc, Indonesia. *Mar. Geol.*, 76:223-241.

Shanmugam, G., and Moiola, R., 1982. Eustatic control of turbidites and winnowed turbidites. *Geology*, 10:231-235.

Shipboard scientific party, 1988. Synthesis of shipboard results: Leg 110 transect of the northern Barbados Ridge. *In* Moore, J. C., and Mascle, A., et al., *Proc. ODP, Init. Repts.*, 110: College Station, TX (Ocean Drilling Program), 577-591.

Southard, J., Young, R., and Hollister, C., 1971. Experimental erosion of calcareous ooze. *J. Geophys. Res.*, 76:5903-5909.

Speed, R. C., and Larue, D. K., 1982. Barbados: Architecture and implications for accretion. *J. Geophys. Res.*, 67:3633-3643.

Stow, D.A.V., and Shanmugam, G., 1980. Sequence of structures in fine-grained turbidites: Comparison of recent deep-sea and ancient flysch sediments. *Sediment. Geol.*, 25: 23-42.

Stow, D.A.V., and Piper, D.J.W., 1982. Deep-water fine-grained sediments: Facies models. In Stow, D., and Piper, D. (Eds.), *Fine-grained sediments: Deep-water processes and facies*: Oxford (Blackwell Scientific Press), 611-646.

Tucholke, B., Hollister, C., Biscaye, P., and Gardner, W., 1985. Abyssal current character determined from sediment bedforms on the Nova Scotian continental rise. *In* Nowell, A., and Hollister, C. (Eds.), *Deep-ocean sediment transport—Preliminary Results of the High Energy Benthic Boundary Layer Experiment. Mar. Geol.*, Spec. Issue, 66:43-58.

Underwood, M. B., 1987. Empirical evidence for upslope flow of turbidity currents in the Aleutian forearc. *Abstr. Programs, Geol. Soc. Am.*, 19:874. (Abstract)

Vail, P., Mitchum, R., Jr., Todd, R., Widmier, J., Thompson, S., III, Sangree, J., Bubb, J., and Hatfield, W., 1977. Seismic stratigraphy and global changes of sea level. *In* Payton, C. (Ed.), Seismic stratigraphy—Applications to hydrocarbon exploration. *AAPG Mem.*, 28: 49-212.

Van Andel, T. H., and Komar, P. D., 1969. Ponded sediments of the Mid-Atlantic Ridge between 22° and 23° North latitude. *Geol. Soc. Am. Bull.*, 80:1163-1190.

Velbel, M. A., 1980. Petrography of subduction zone sandstones—Discussion. *J. Sediment. Petrol.*, 50:303-304.

Weatherly, G., and Kelley, E., 1985. Storms and flow reversals at the HEBBLE site. *In* Nowell, A., and Hollister, C. (Eds.), *Deep-sea sediment transport—Preliminary results of the High Energy Benthic Boundary Layer Experiment. Mar. Geol.*, Spec. Issue, 66:205-218.

Westbrook, G. K., Mascle, A., and Biju-Duval, B., 1984a. Geophysics and the structure of the Lesser Antilles forearc. *In* Moore, J. C., and Biju-Duval, B. (Eds.), *Init. Repts. DSDP*, 78A: Washington, D. C. (U. S. Govt. Printing Office), 23-38.

Westbrook, G. K., Mauffret, A., Munschy, M., Jackson, R., Biju-Duval, B., Mascle, A., and Ladd, J. W., 1984b. Depth to acoustic basement. *In* Speed, R. C., Westbrook, G. K., and others (Eds.), Lesser Antilles arc and adjacent terranes. *Atlas 10, Ocean Margin Drilling Program Regional Atlas Series*, Woods Hole, MA (Marine Science International).

Date of initial receipt: 11 March 1988
Date of acceptance: 31 March 1989
Ms 110B-124

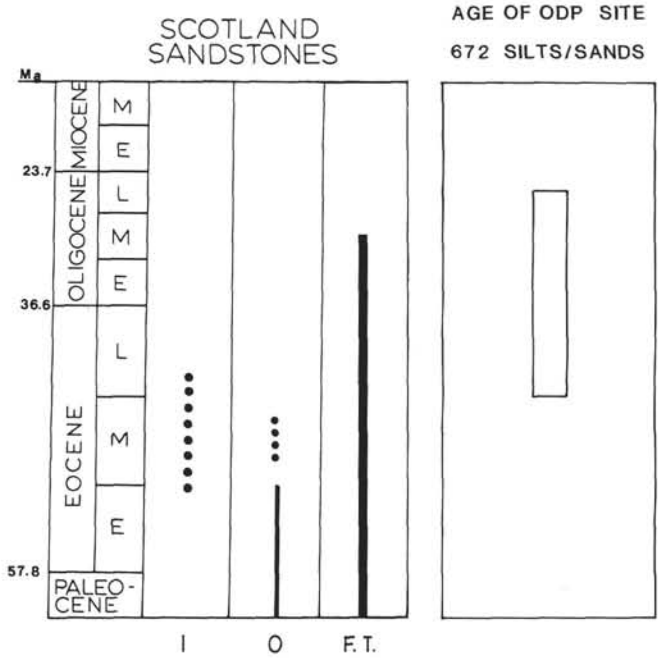

Figure 13. Comparison of ages of ODP Leg 110 terrigenous sediments and Scotland Group sandstones from Barbados (from Baldwin et al., 1986). The two left columns (1 and 0) show biostratigraphic ages determined for the Scotland Group at different localities (after Speed and Larue, 1982). The right-hand column (F. T.) represents fission track ages derived from Scotland Group zircons by Baldwin et al (1986). Although the youngest fission-track ages shown on the diagram are 30 Ma, some samples yielded ages as young as 25 Ma (Baldwin et al., 1986). These ages suggest that the microfossils used in the biostratigraphic dating of Scotland Group sandstones may be reworked. The far-right column shows biostratigraphic ages of the terrigenous sediments in the ODP Leg 110 area. Note the similarity in minimum ages between the ODP sediments and the Scotland Group fission-track ages of Baldwin et al. (1986).

APPENDIX: ODP LEG 110 GRAIN-SIZE ANALYSIS METHODS

The particle-size distributions of selected samples from beneath, within, and above suspected turbidites was determined for 98 samples from middle Eocene-upper Oligocene deposits recovered during ODP Leg 110. Sample size was approximately 0.5 cm^2. Samples were dispersed in 200 mL of Calgon solution, stirred, and placed in an ultrasonic cleaner for 2 min. After it settled for 2 hr the Calgon solution was decanted. This step was repeated twice. 200 mL of distilled water was then added to the sediment, stirred, allowed to settle for 2 hr, and then decanted. Grain-size frequency distributions (volume percent vs. phi grain size units) and mean grain sizes (in phi units) were obtained by placing a sample in an Elzone electronic sizing instrument. Analytical precision of this instrument is ± 0.05 phi units. A full description of the particle-size analysis method is given in Blaeser and Ledbetter (1982). Orifice size on the particle counter determines the range of sizes analyzed. Each orifice only records a grain-size range of 1.5-50% of the orifice diameter. For example, a 120-μm orifice will record grain sizes of 2-4 to 60 μm. Due to the wide range of grain sizes analyzed from the Leg 110 sediments, we used several different orifice sizes: A 380-μm orifice for medium silt to fine sand, a 240-μm orifice for fine silt to very fine sand, and a 120-μm orifice for very fine silt to coarse silt. However, the same orifice was used for all samples within each bed. In beds where the larger orifices were used, the apparent grain size of the finest-grained portions of the beds (e.g., clay) is shown as being artificially coarse.

EXPLANATION OF GRAIN-SIZE PLOTS

Grain-size frequency distributions (volume percent vs. grain size), and plots of mean grain sizes (mean grain size vs. depth in core) are provided for each bed. All samples are from ODP Hole 672A except 110-674A-29-CC. Lithology of each interval is shown below each mean grain-size plot: T = terrigenous bed, C = clay bed, and M = marl bed. Grain-size scale (vertical) on mean grain-size plots is not the same between diagrams. Grain-size trends (e.g., graded bedding) are shown connected by solid lines within individual beds, as defined by visual core descriptions. Arrows at the ends of some of the solid connecting lines indicate that these beds continue into an adjacent core or section.

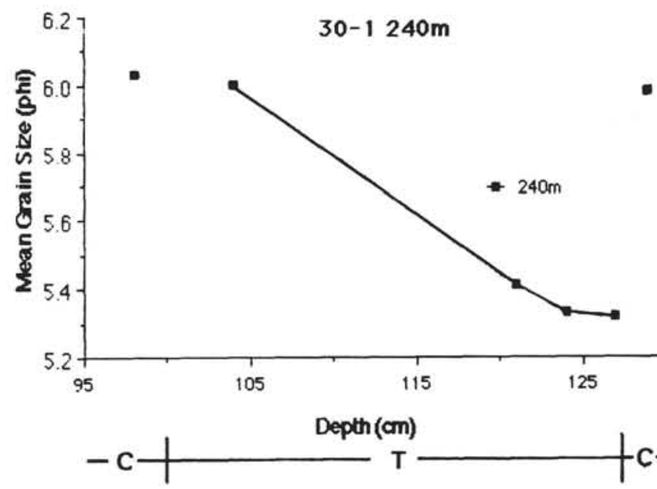

APPENDIX (continued).

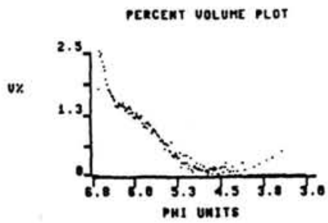

30-1 98.0 240m

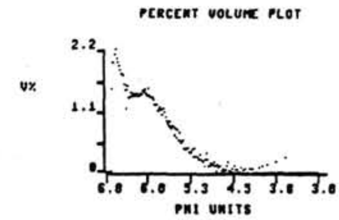

30-1 104.5 240m

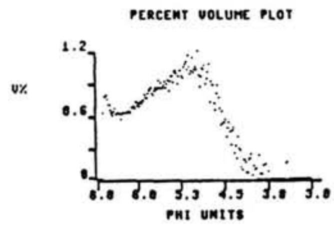

30-1 121.0 240m

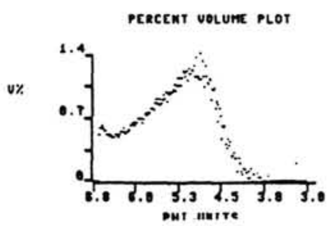

30-1 124.0 240m

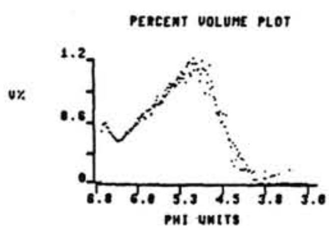

30-1 127.3 240m

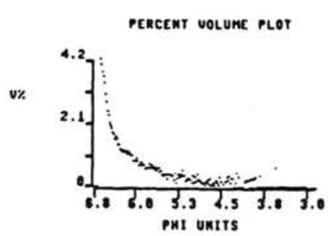

30-1 128.0 240m

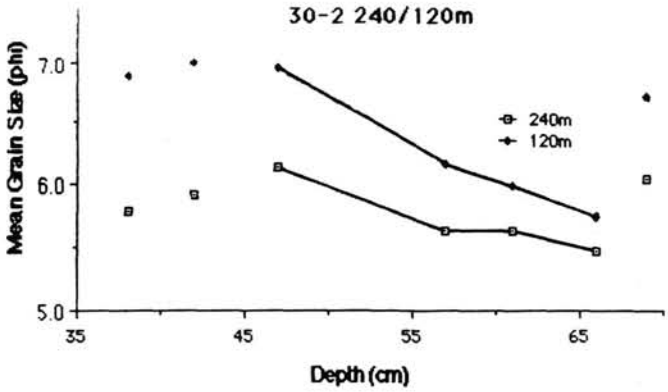

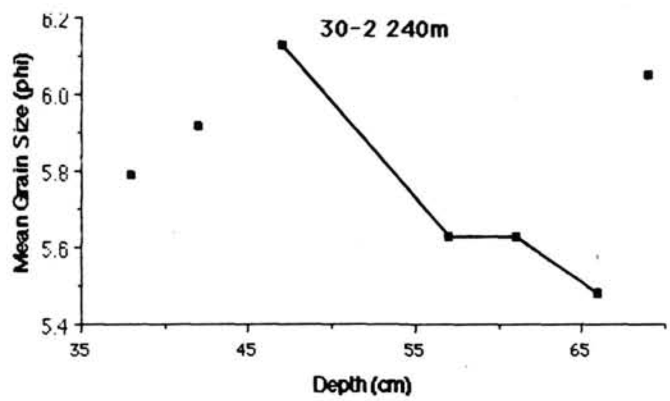

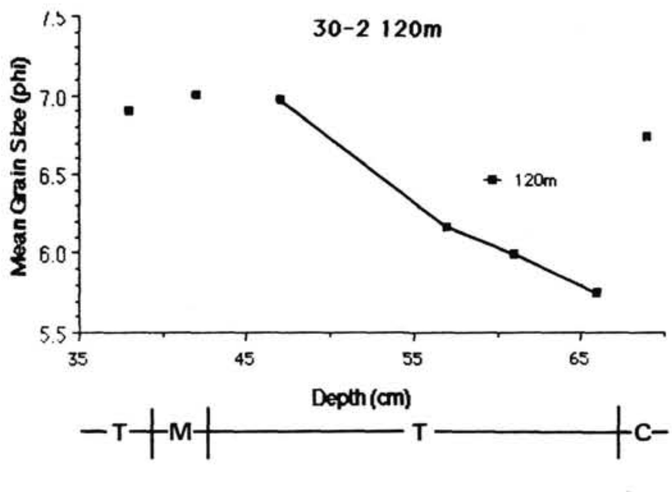

APPENDIX (continued).

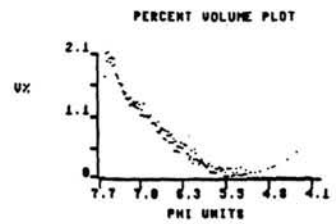

30-2 38.0 120m

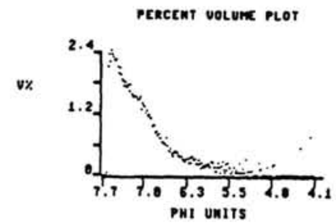

30-2 41.6 120m

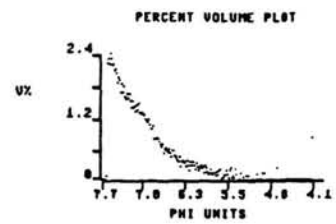

30-2 46.7 120m

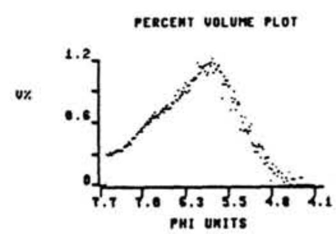

30-2 57.2 120m

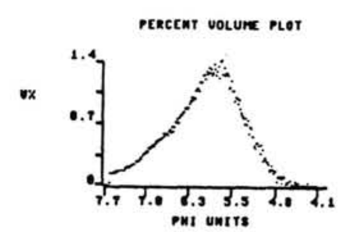

30-2 61.5 120m

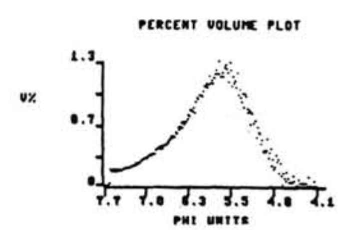

30-2 66.0 120m

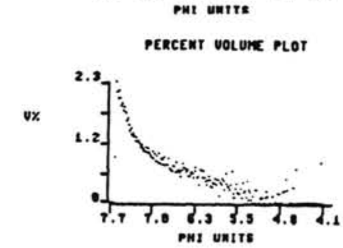

30-2 69.0 120m

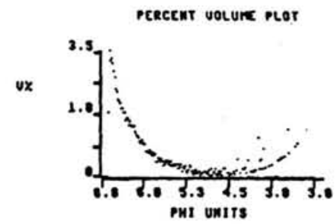

30-2 38.0 240m

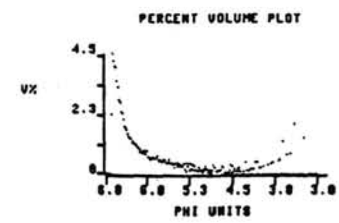

30-2 41.6 240m

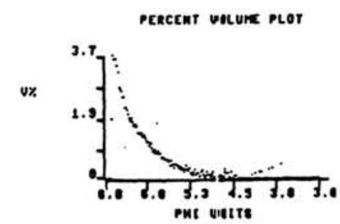

30-2 46.7 240m

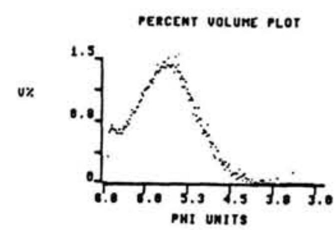

30-2 57.2 240m

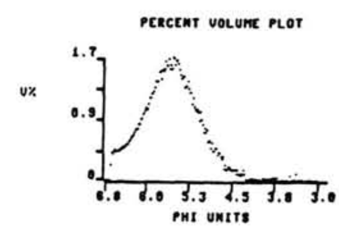

30-2 61.5 240m

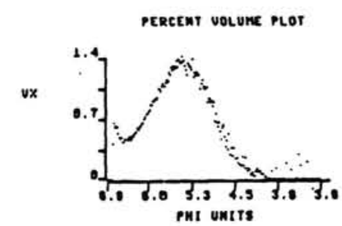

30-2 66.0 240m

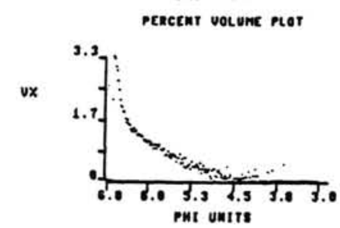

30-2 69.0 240m

APPENDIX (continued).

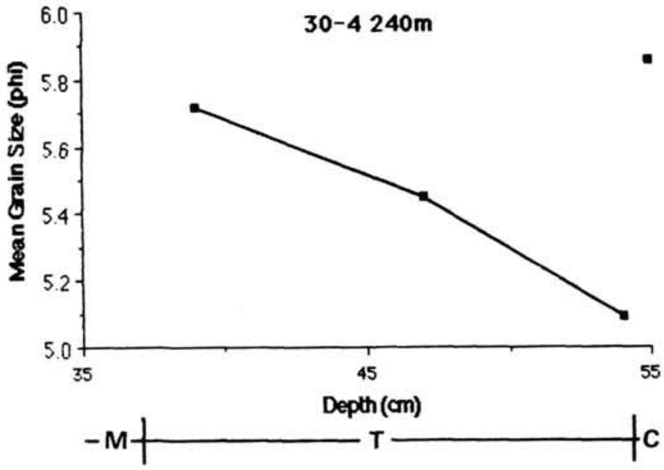

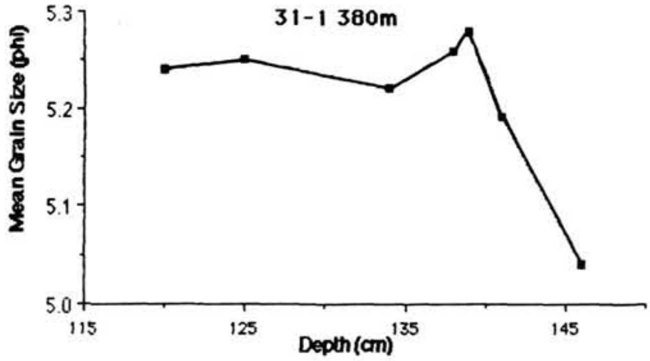

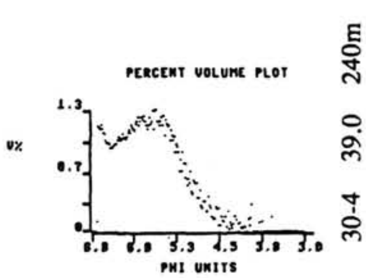

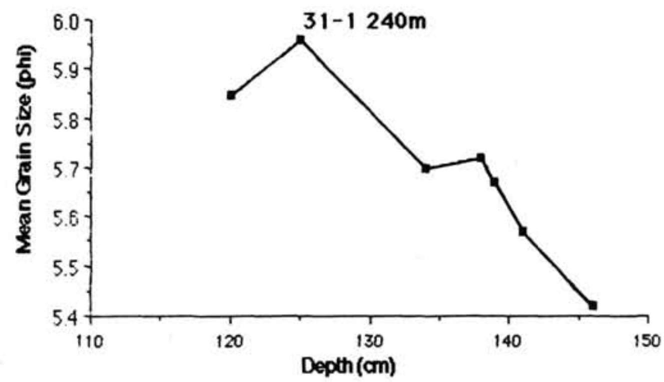

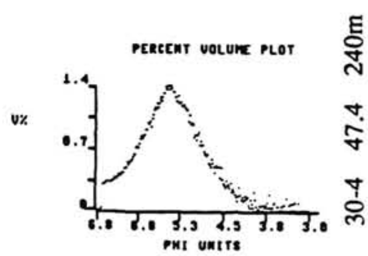

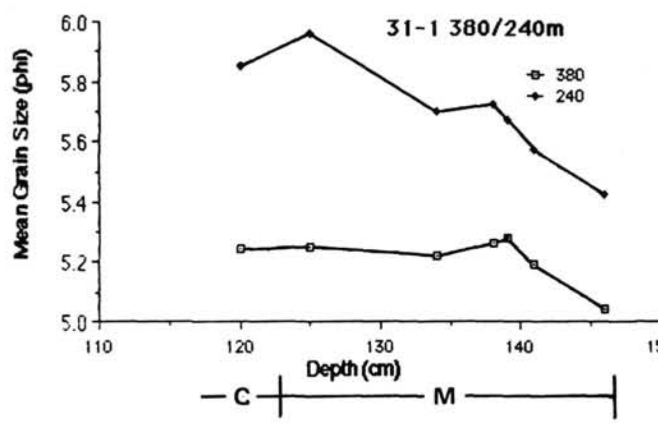

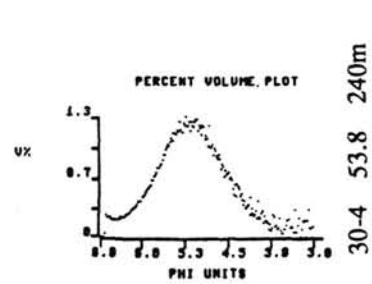

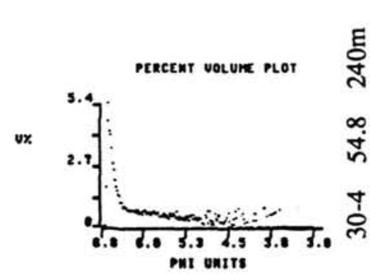

APPENDIX (continued).

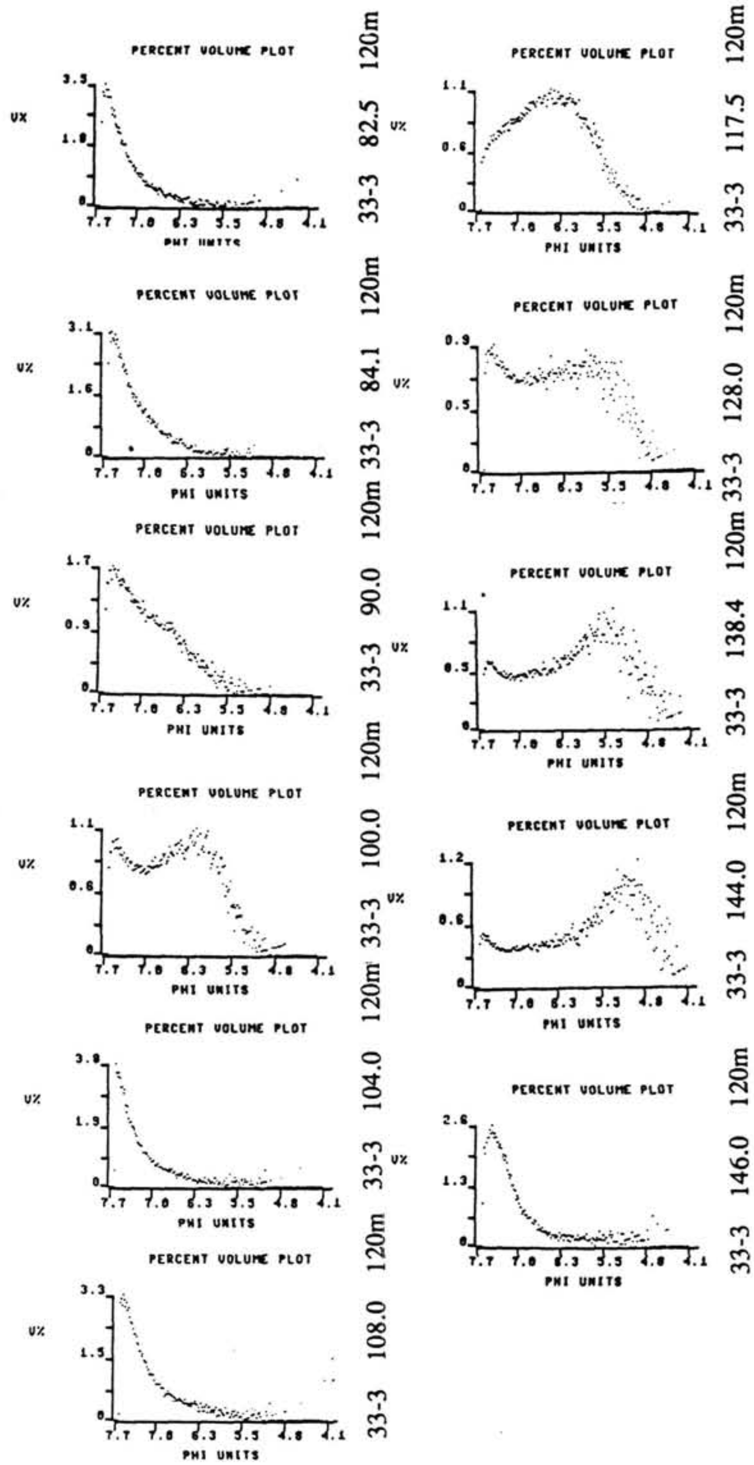

APPENDIX (continued).

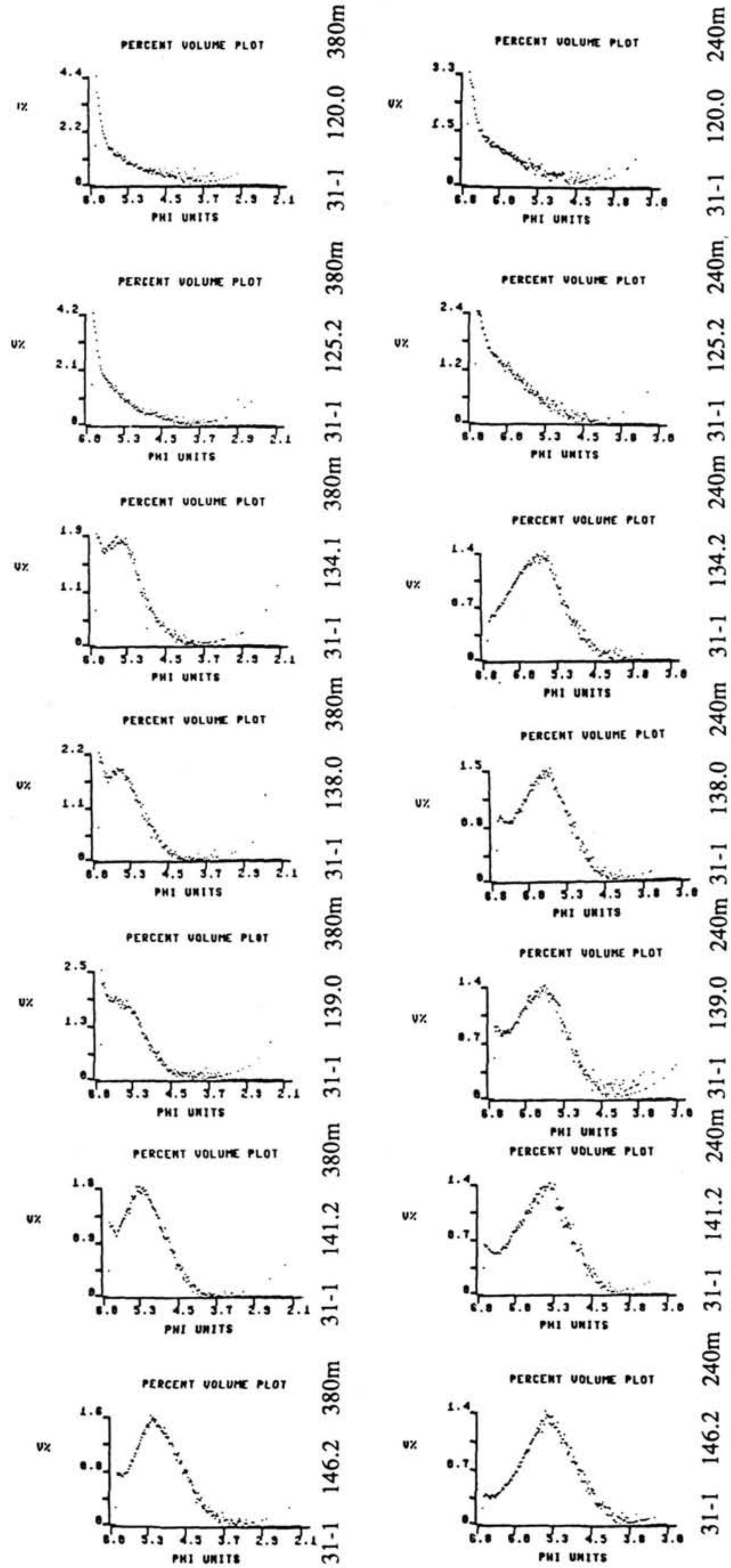

APPENDIX (continued).

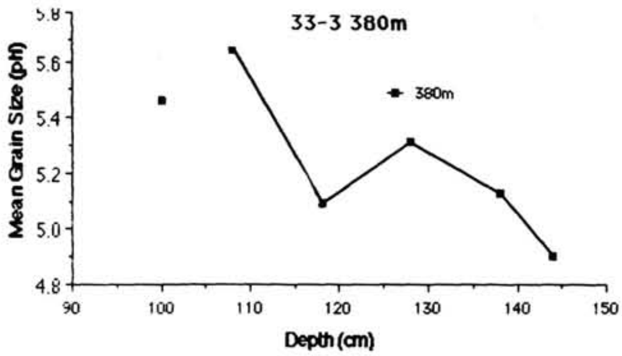

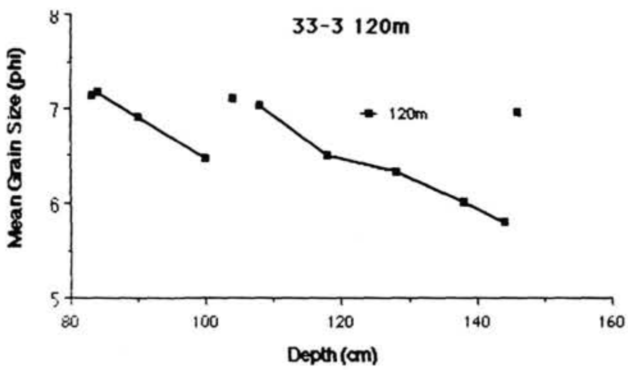

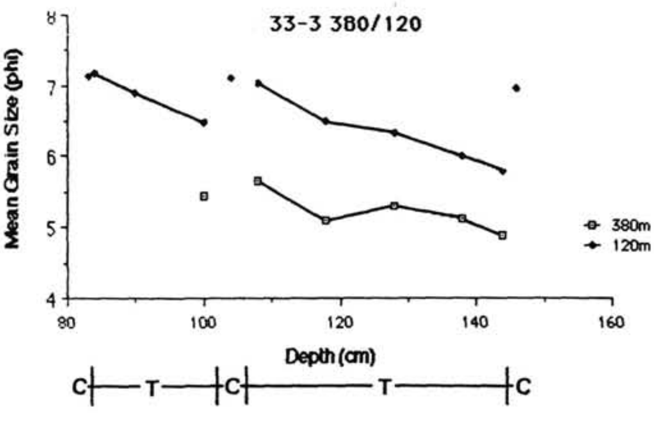

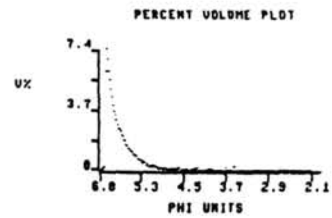

33-3 90.0 380m

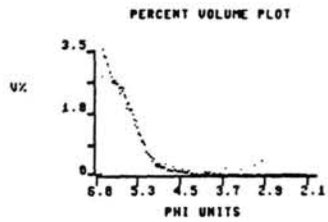

33-3 100.0 380m

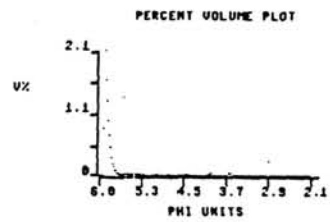

33-3 107.5 380m

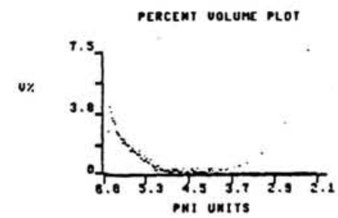

33-3 117.5 380m

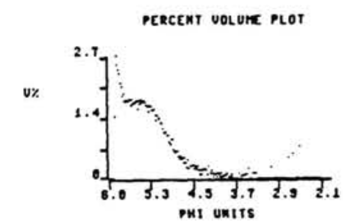

33-3 128.0 380m

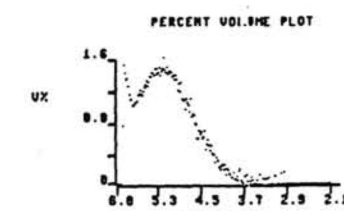

33-3 138.4 380m

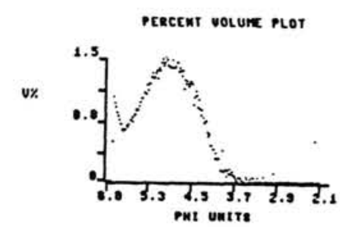

33-3 144.0 380m

APPENDIX (continued).

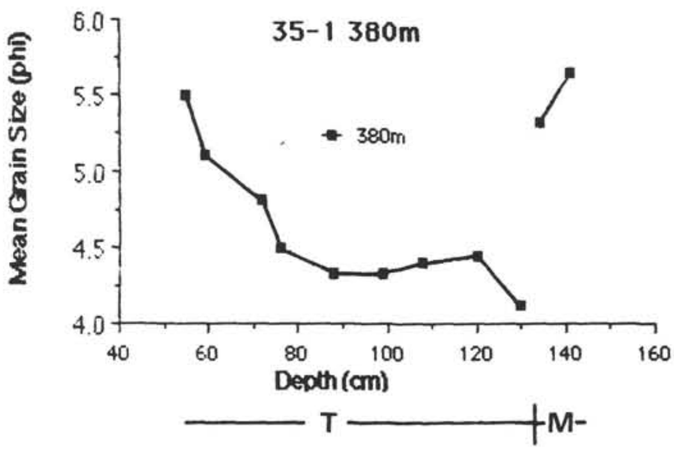

APPENDIX (continued).

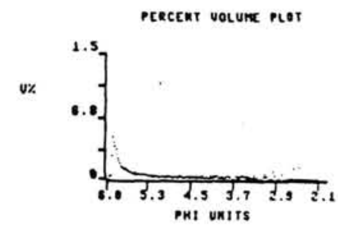

35-1 37.8 380m

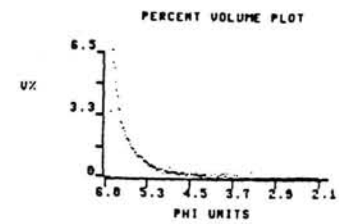

35-1 54.5 380m

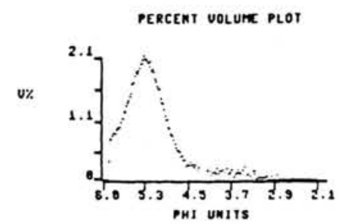

35-1 58.8 380m

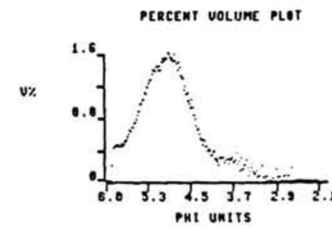

35-1 72.2 380m

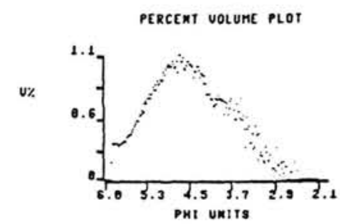

35-1 75.6 380m

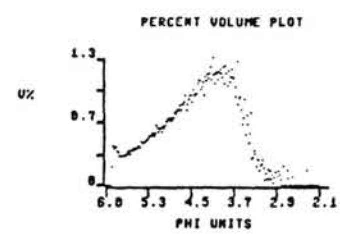

35-1 88.0 380m

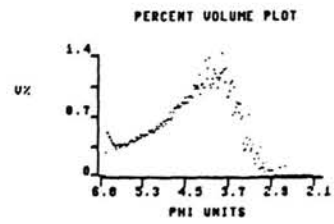

35-1 98.5 380m

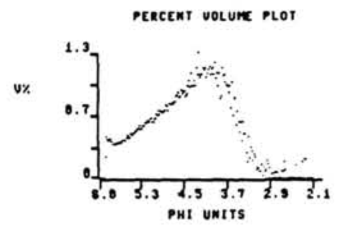

35-1 107.8 380m

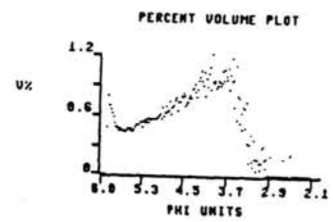

35-1 120.0 380m

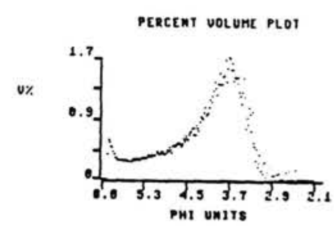

35-1 129.6 380m

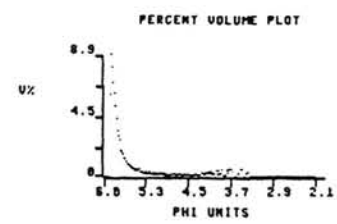

35-1 134.0 380m

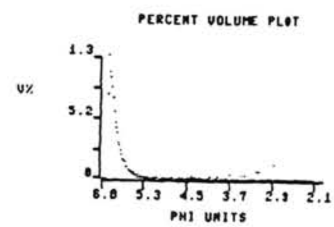

35-1 141.0 380m

APPENDIX (continued).

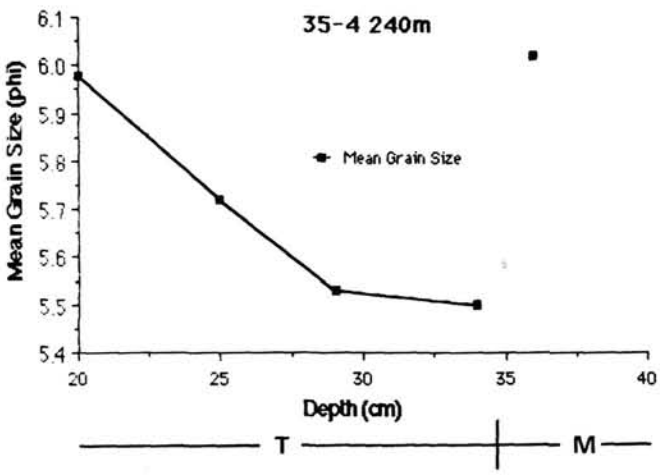

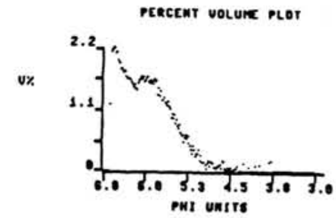

35-4 19.8 240m

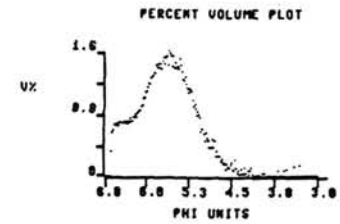

35-4 25.3 240m

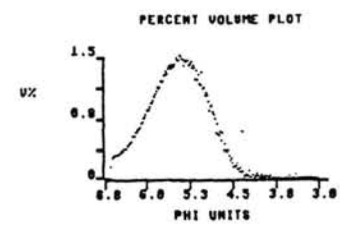

35-4 29.2 240m

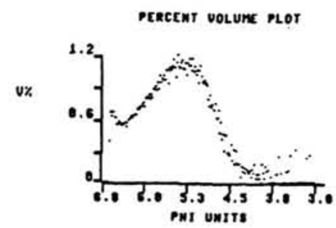

35-4 33.5 240m'

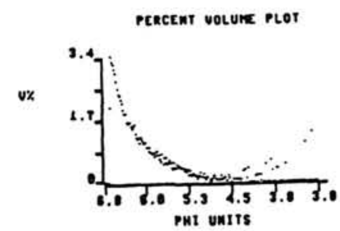

35-4 36.2 240m

APPENDIX (continued).

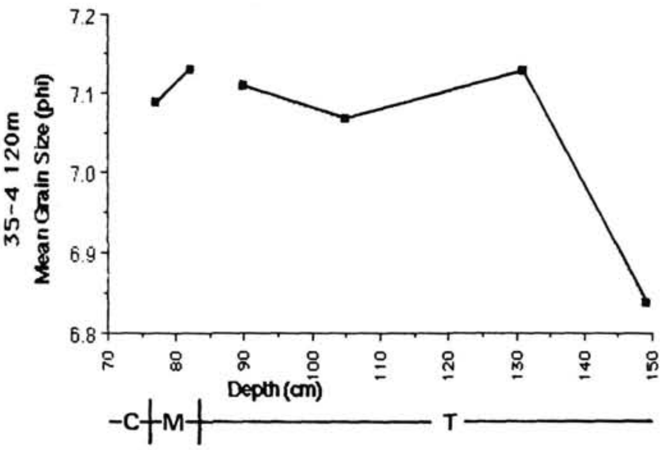

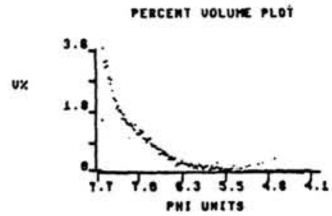

35-4 77.5 120m

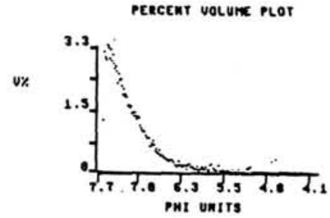

35-4 82.5 120m

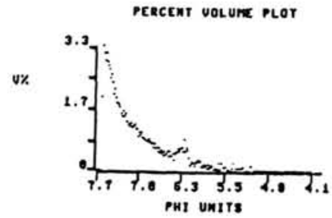

35-4 90.5 120m

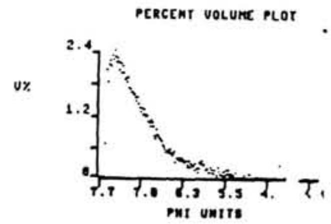

35-4 105.5 120m

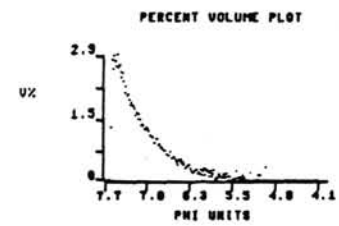

35-4 130.5 120m

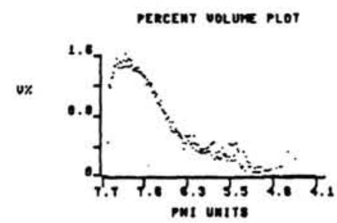

35-4 149.1 120m

APPENDIX (continued).

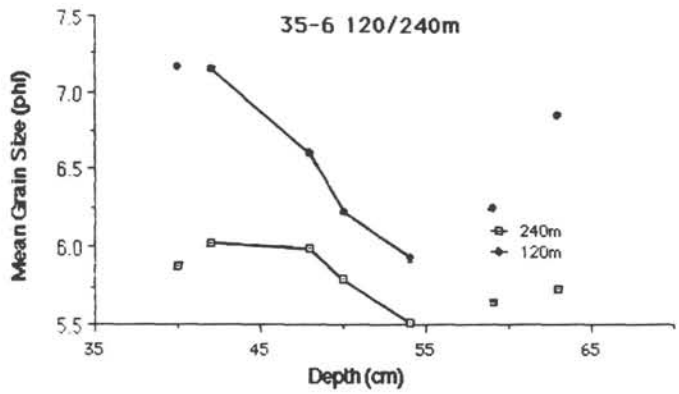

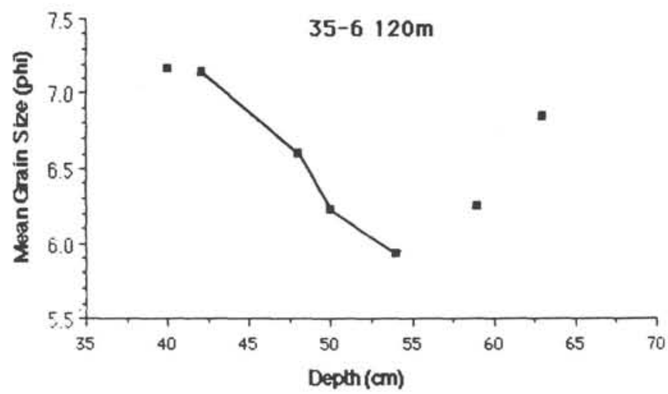

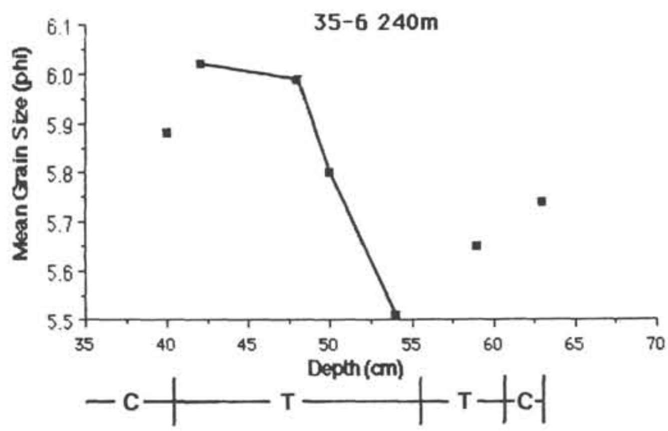

APPENDIX (continued).

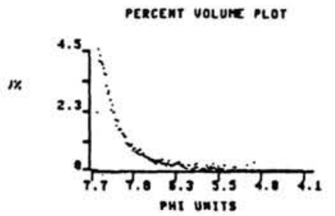

35-6 40.0 120m

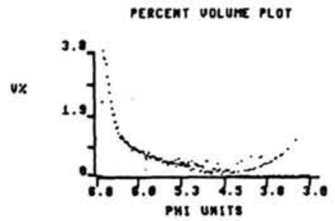

35-6 40.0 240m

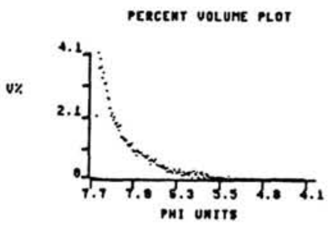

35-6 42.0 120m

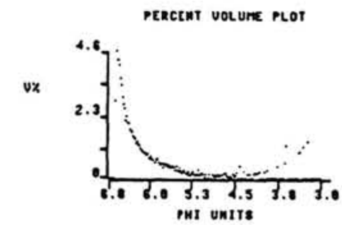

35-6 42.0 240m

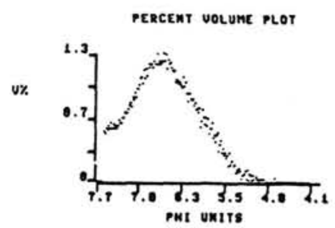

35-6 48.0 120m

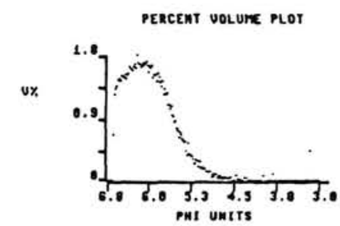

35-6 48.0 240m

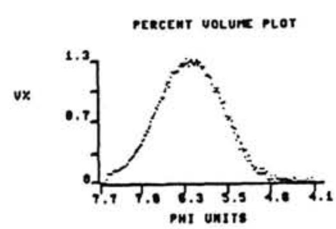

35-6 50.5 120m

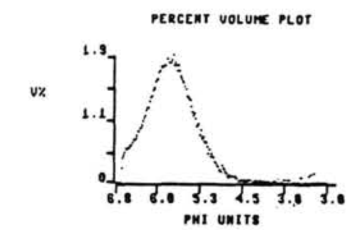

35-6 50.5 240m

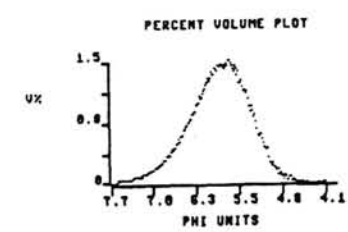

35-6 54.4 120m

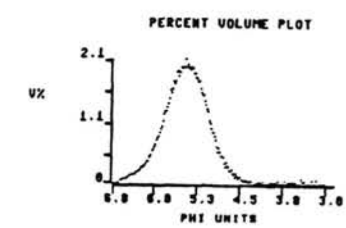

35-6 54.4 240m

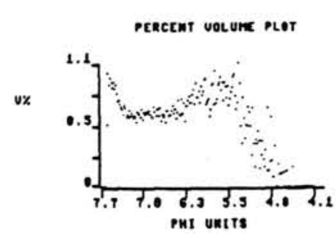

35-6 58.7 120m

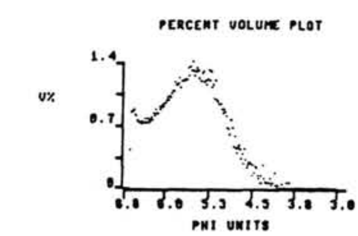

35-6 58.7 240m

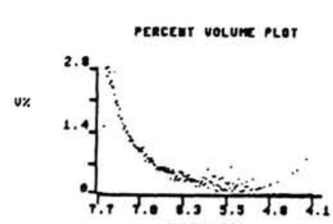

35-6 62.5 120m

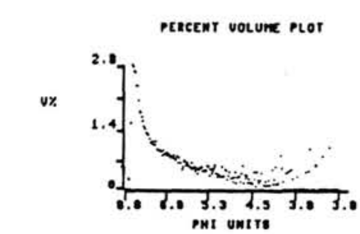

35-6 62.5 240m

APPENDIX (continued).

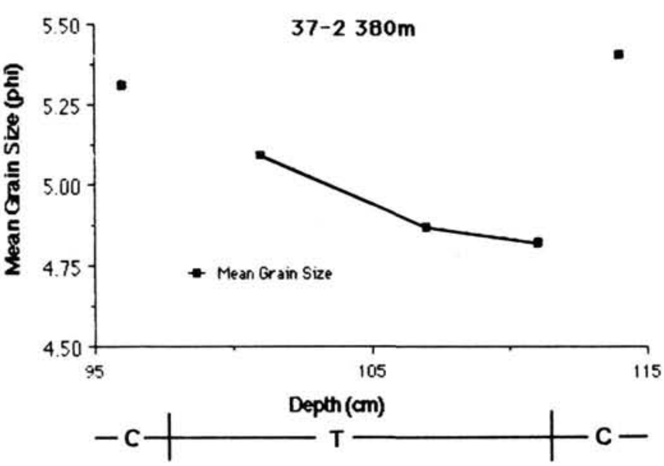

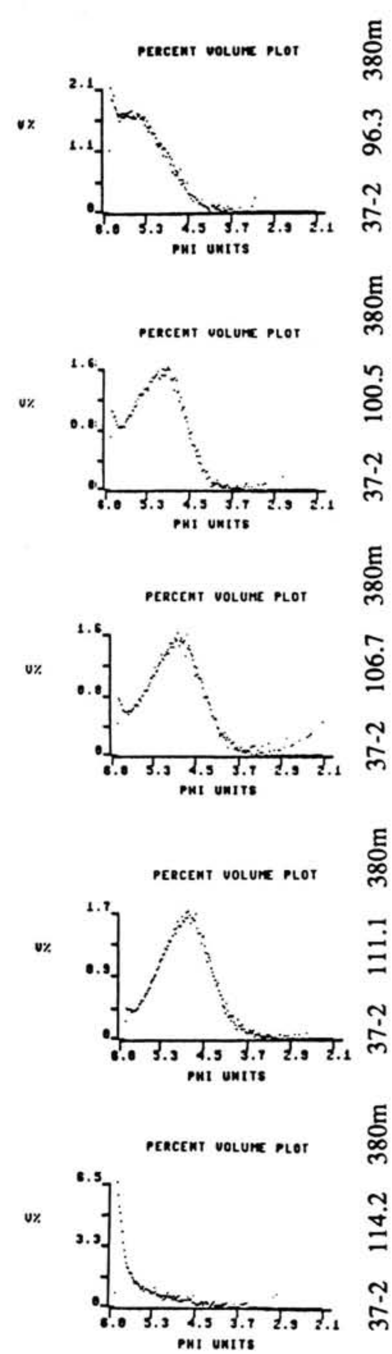

APPENDIX (continued).

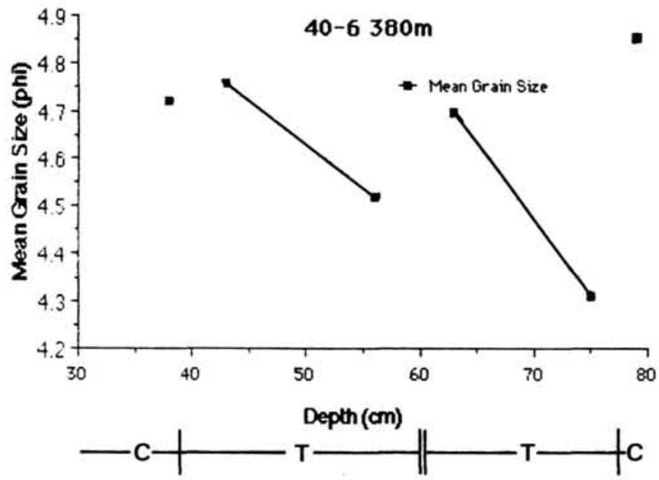

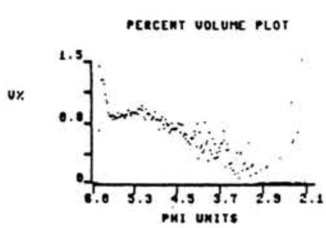

40-6 38.0 380m

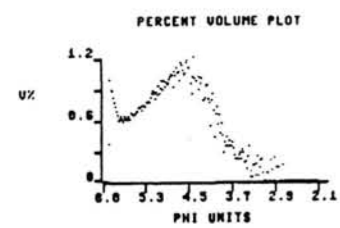

40-6 62.8 380m

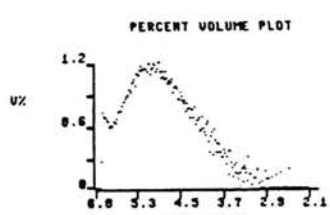

40-6 43.2 380m

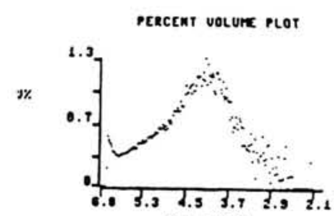

40-6 75.0 380m

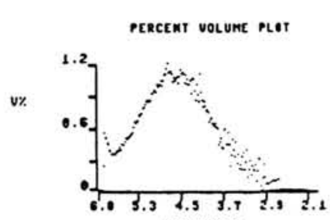

40-6 56.2 380m

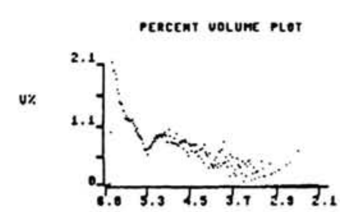

40-6 79.0 380m

APPENDIX (continued).

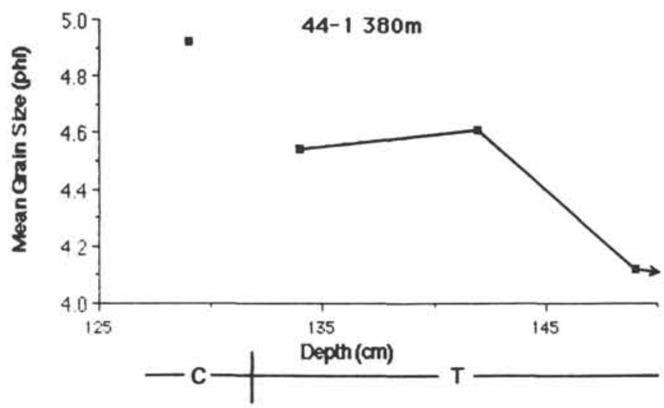

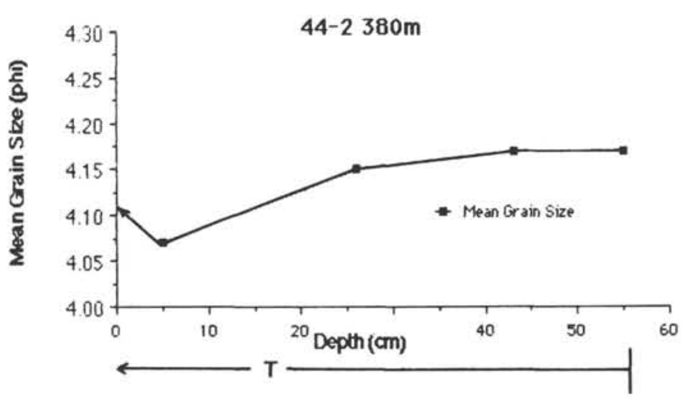

APPENDIX (continued).

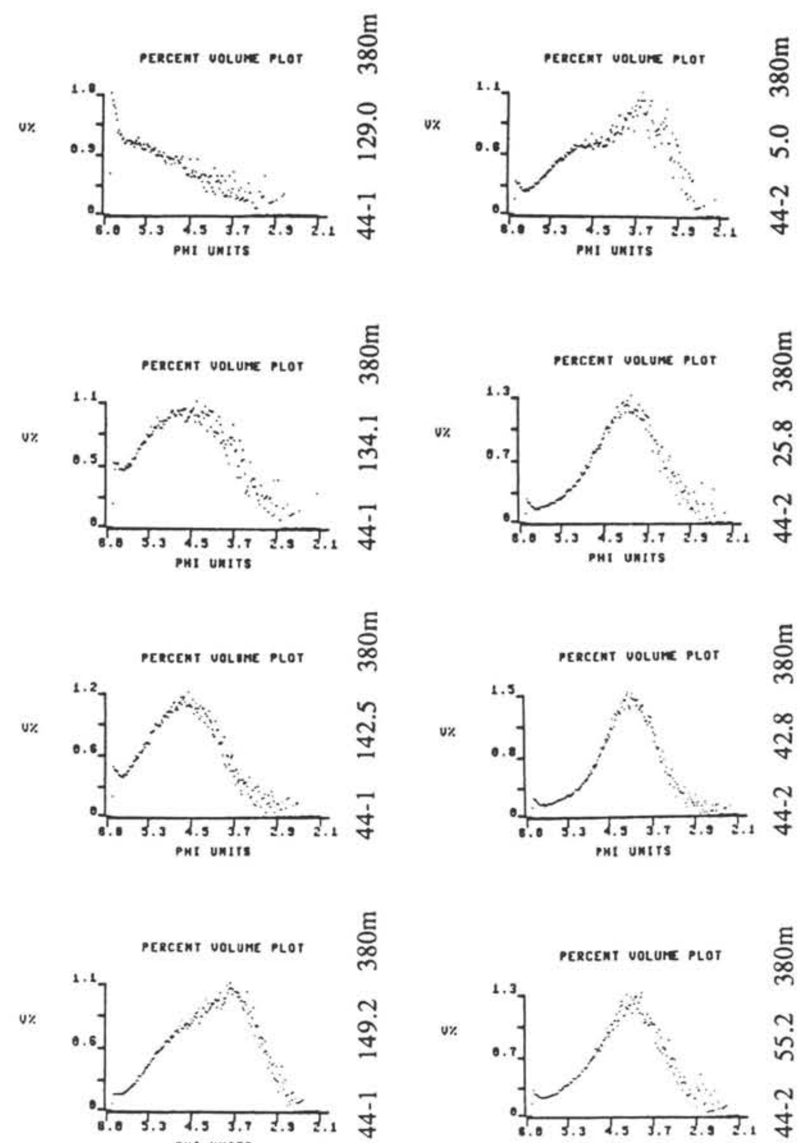

APPENDIX (continued).

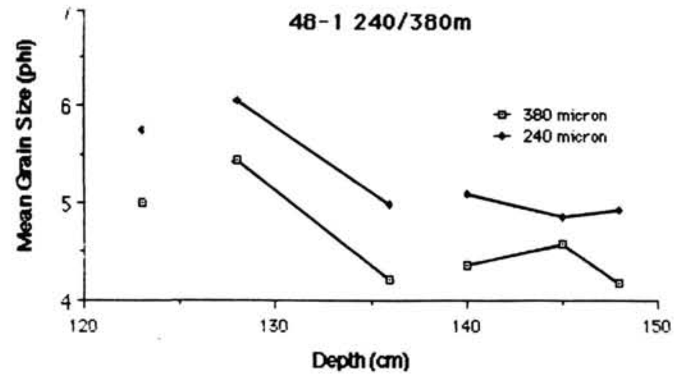

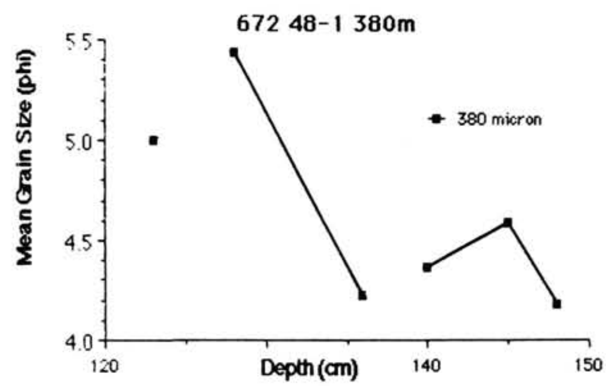

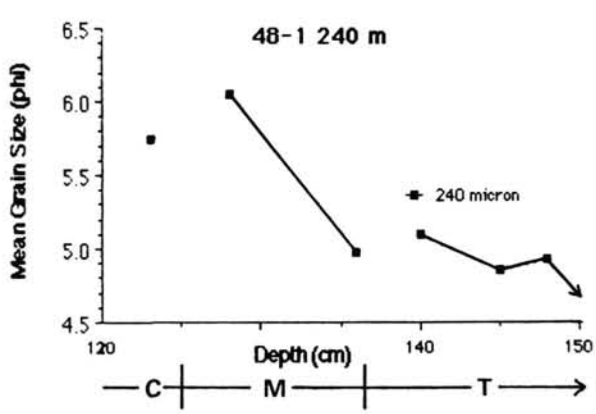

APPENDIX (continued).

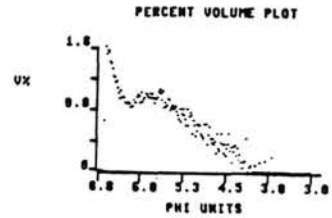

48-1 123.4 240m

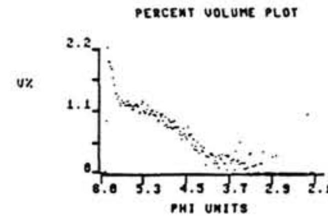

48-1 123.4 380m

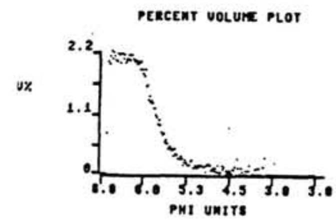

48-1 127.8 240m

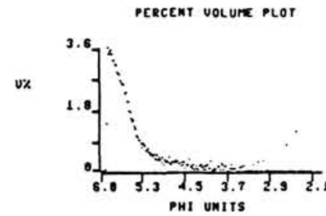

48-1 127.8 380m

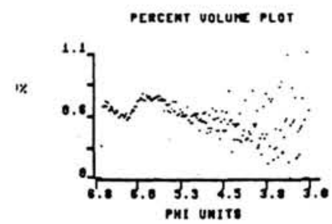

48-1 136.0 240m

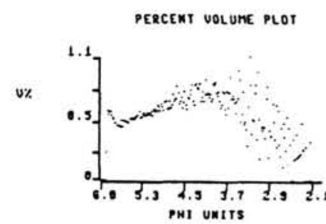

48-1 136.0 380m

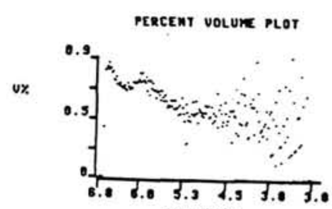

48-1 140.0 240m

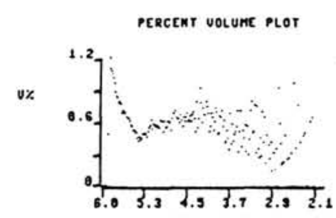

48-1 140.0 380m

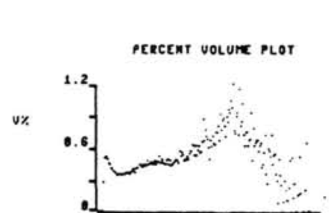

48-1 144.7 240m

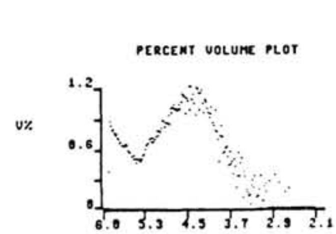

48-1 144.7 380m

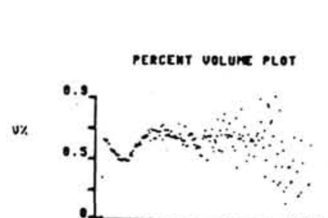

48-1 148.8 240m

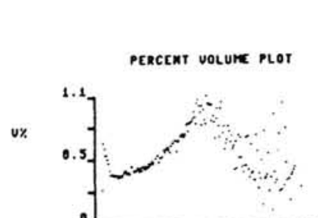

48-1 148.8 380m

APPENDIX (continued).

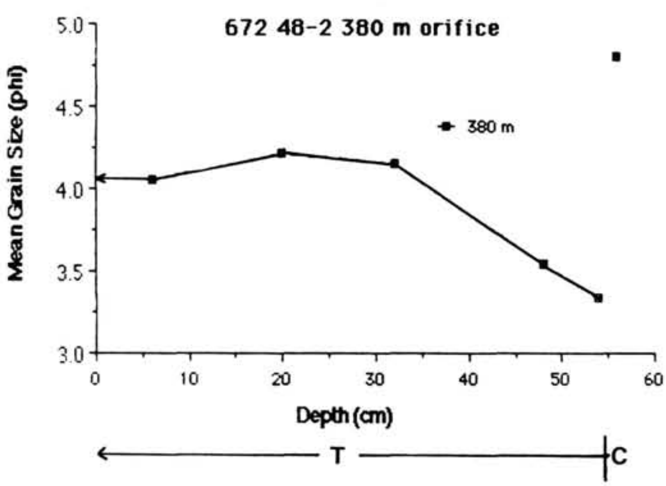

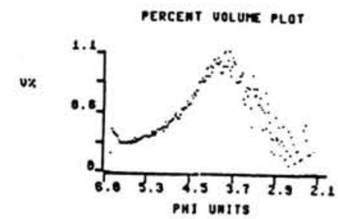

48-2 6.0 380m

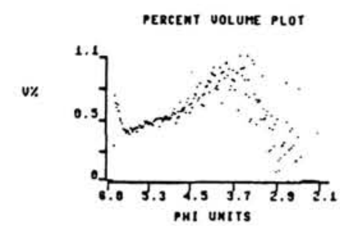

48-2 20.0 380m

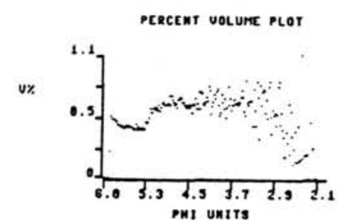

48-2 31.8 380m

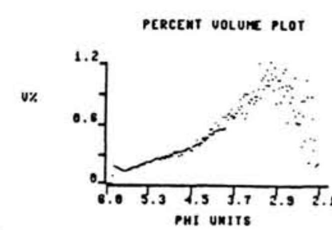

48-2 48.0 380m

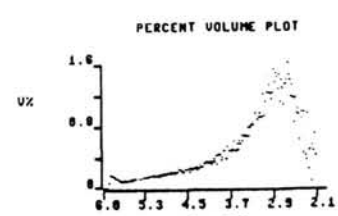

48-2 53.8 380m

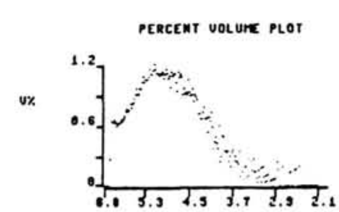

48-2 56.0 380m

APPENDIX (continued).

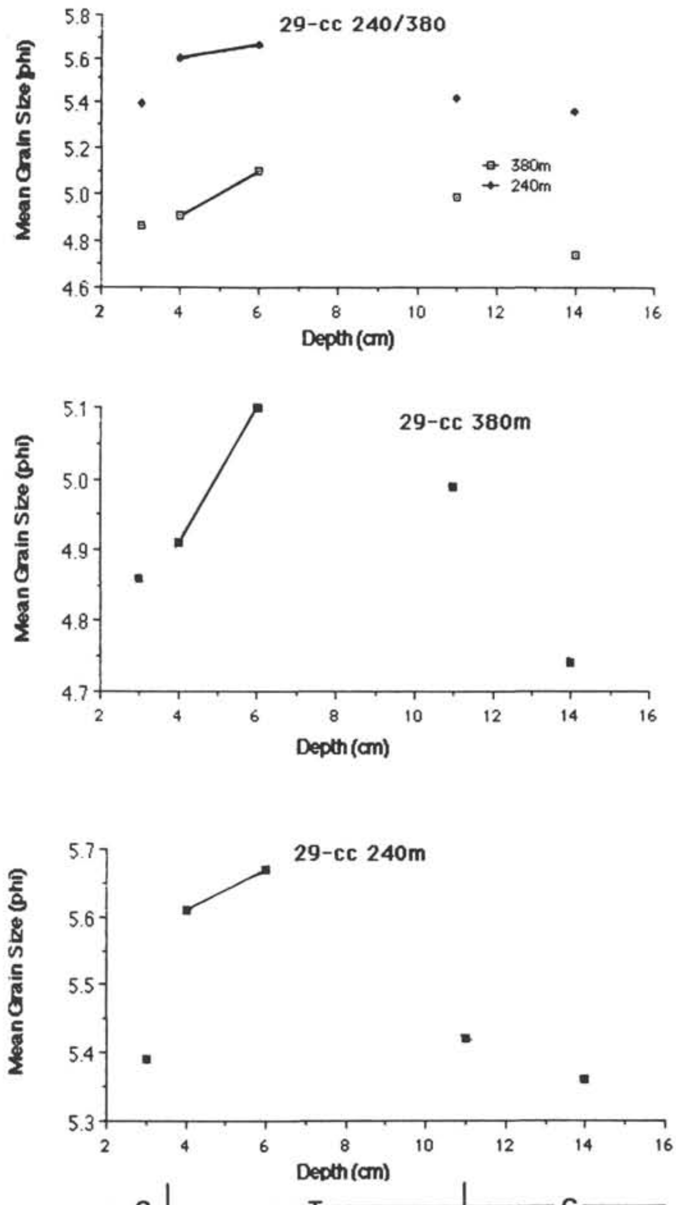

HOLE 674A: OVERTURNED

APPENDIX (continued).

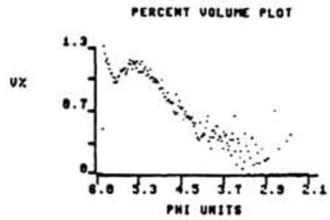

29CC 3.0 380m

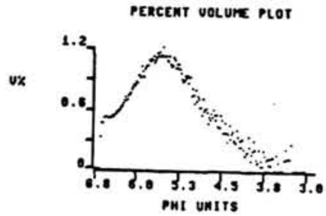

29CC 3.0 380m

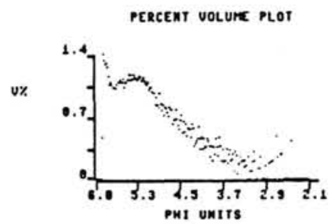

29CC 4.0 380m

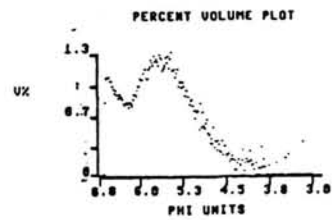

29CC 4.0 380m

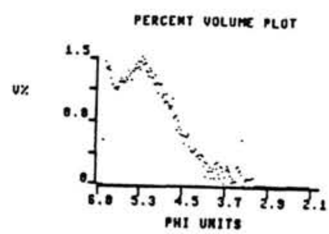

29CC 6.1 380m

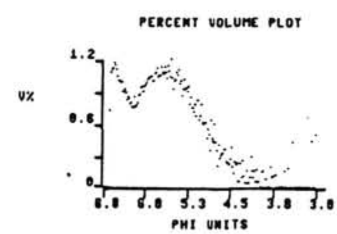

29CC 6.1 380m

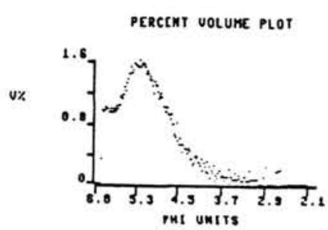

29CC 10.5 380m

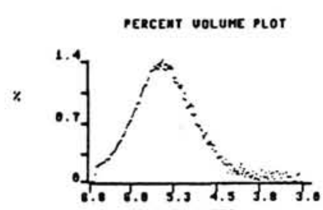

29CC 10.5 380m

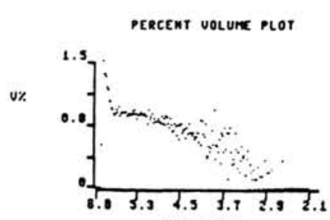

29CC 14.1 380m

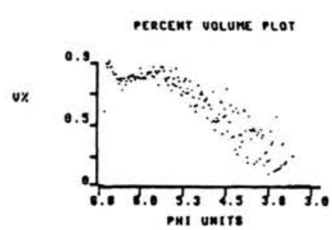

29CC 14.1 380m